Suppression without inhibition: A novel mechanism in the retina accounts for saccadic suppression

Saad Idrees[1,2], Matthias-Philipp Baumann[1], Maria M. Korympidou[1,2,3], Timm Schubert[1,3], Alexandra Kling[4], Katrin Franke[3,5], Ziad M. Hafed[1], Felix Franke[6,7,8]∗, Thomas A. Münch[1,3]∗

[1]Werner Reichardt Centre for Integrative Neuroscience, University of Tübingen, 72076 Tübingen, Germany

[2]International Max Planck Research School, University of Tübingen, 72074 Tübingen, Germany

[3]Institute for Ophthalmic Research, University of Tübingen, 72076 Tübingen, Germany

[4]Department of Neurosurgery, Stanford School of Medicine, Stanford, CA 94305, USA

[5]Bernstein Center for Computational Neuroscience, University of Tübingen, 72076 Tübingen, Germany

[6]Bio Engineering Laboratory, ETH Zürich, 4058 Basel, Switzerland

[7]Institute of Molecular and Clinical Ophthalmology Basel, 4031 Basel, Switzerland

[8]Faculty of Science, University of Basel, 4056 Basel, Switzerland

∗Correspondence: felfranke@googlemail.com (F.F.), thomas.muench@gmail.com (T.A.M.)

Abstract

Visual perception remains stable across saccadic eye movements, despite the concurrent strongly disruptive visual flow. This stability is partially associated with a reduction in visual sensitivity, known as saccadic suppression, which already starts in the retina with reduced ganglion cell sensitivity. However, the retinal circuit mechanisms giving rise to such suppression remain unknown. Here, we describe these mechanisms using electrophysiology in mouse, pig, and macaque retina, 2-photon calcium imaging, computational modeling, and human psychophysics. We find a novel retinal processing motif underlying retinal saccadic suppression, “dynamic reversal suppression”, which is triggered by sequential stimuli containing contrast reversals. This motif does not involve inhibition but relies on nonlinear transformation of the inherently slow responses of cone photoreceptors by downstream retinal pathways. Two further components of suppression are present in ON ganglion cells and originate in the cells’ receptive field surround, highlighting a novel disparity between ON and OFF ganglion cells. Our results are relevant for any sequential stimulation encountered frequently in naturalistic scenarios.

Keywords: retina, ganglion cell, cone photoreceptor, saccadic suppression, computational model, sequential stimuli, rapid image shifts, perception, dynamic vision, visual processing

Introduction

Vision appears as a continuous and coherent process. This is a striking achievement of the visual system, considering that the visual flow acrsoss the retina is not continuous, but governed by frequent and sudden changes, irregularities, and disruptions. As a consequence of this active vision, i.e. the process of active exploration of the visual environment, the meaningful images falling onto the retina are only brief snapshots of the world, interrupted by blinks and rapid motion. The most prominent cause for such disruptions are eye movements. Saccades, for example, are critical for efficiently sampling the visual world (Schütz et al., 2011; Tatler et al., 2010; Yarbus, 1967), which is particularly true for species in which high visual resolution is limited to a small fraction of the overall visual space, such as the foveal region in primates. On the other hand, as a result of saccades, the number of photons falling onto a given area of the retina can change by several orders of magnitude within tens of milliseconds, causing sudden and frequent visual transients of local intensity across the entire retina. From the perspective of the retina, saccades are therefore equivalent to robust visual stimuli, and they are a powerful model for a very profound question of visual neuroscience: How does the visual system extract robust information from the "meaningful" snapshots of the world, in the face of frequent, strong, and disruptive other input?

Perceptually, saccadic disruptions are minimized by reducing the sensitivity of the visual system to new input around the time of saccades - a phenomenon known as saccadic suppression. While this phenomenon has been extensively characterized over the past few decades (Beeler, 1967; Bremmer et al., 2009; Idrees et al., 2020; Krekelberg, 2010; Matin, 1974; Volkmann, 1986; Wurtz, 2008; Zuber and Stark, 1966), its underlying mechanisms still remain unclear. Several electrophysiological studies have shown neural correlates of saccadic suppression throughout the visual system, namely a modulation of neural activity and/or sensitivity around the time of saccades (Bremmer et al., 2009; Chen and Hafed, 2017; Hafed and Krauzlis, 2010; Ibbotson et al., 2008; Kleiser et al., 2004; Krekelberg, 2010; Wurtz, 2008). These observations have often been interpreted to be caused by active suppressive signals originating from (pre-) motor areas, such as corollary discharge signals related to the saccadic eye movement command (Bremmer et al., 2009; Diamond et al., 2000; Duffy and

Lombroso, 1968; Ross et al., 2001; Zuber and Stark, 1966). Most studies investigating the mechanisms of saccadic suppression have therefore focused on cortical or subcortical neuronal recordings and/or on behavioral measures of perceptual state, largely neglecting the consequence of visual processing in early visual pathways, for example in the retina.

The retina is an independent signal processing “front end” in the visual system, before visual information is sent along the optic nerve to higher brain areas. Consequently, image processing triggered by visual transients, such as those that naturally occur during active vision, including saccades, could potentially lead to altered retinal output. Retinal signal processing could therefore contribute to perceptual saccadic suppression. Some studies have investigated how the retina processes information in the context of spatio-temporal dynamics that occur during natural visual behavior (Appleby and Manookin, 2019; Baccus et al., 2008; Berry et al., 1999; Chen et al., 2013; Fried et al., 2002; Garvert and Gollisch, 2013; Geffen et al., 2007; Gollisch, 2013; Münch et al., 2009; Tikidji-Hamburyan et al., 2015; Wei, 2018; Zaghloul et al., 2007; Zhang et al., 2012), including saccades (Amthor et al., 2005; Barlow et al., 1977; Enroth-Cugell and Jakiela, 1980; Krishnamoorthy et al., 2017; Krueger and Fischer, 1973; Noda and Adey, 1974; Passaglia et al., 2009; Roska and Werblin, 2003). A retinal neural correlate of perceptual saccadic suppression has recently been shown by a previous study from our labs (Idrees et al., 2020). There, we showed that the retinal output is indeed altered by saccade-like image shifts. In most mouse and pig retinal ganglion cells (RGCs) that we recorded from, responses to brief probe flashes were suppressed when preceded by saccade-like image displacements across the retina. This retinal saccadic suppression had properties consistent with the perceptual suppression of probe flashes reported by human subjects using similar images, and following either real or simulated saccades. In fact, we already observed elementary properties of perceptual saccadic suppression, such as its dependency on background scene statistics, at the level of the output of the retina, providing strong evidence of a retinal mechanism directly contributing to perceptual saccadic suppression.

In this study, we describe such a mechanism. We experimentally mimicked the visual flow resulting from saccades and recorded the neural activity of the output neurons of the retina (RGCs) from ex vivo retinae of mice, pigs, and macaque monkeys. We found

that retinal saccadic suppression was the result of multiple mechanisms. The major component originated from a novel visual processing motif within an RGC's receptive field center, which we call "dynamic reversal suppression". Dynamic reversal suppression does not depend on any inhibitory signals; it results from a combination of inherent response properties of cone photoreceptors and non-linear processing of cone output by downstream pathways in the retina. Two further components of suppression originated from beyond the RGC's receptive field center, only one of them driven by GABAergic inhibition. Interestingly, these two additional components were observed primarily in ON RGCs, highlighting a novel disparity between ON and OFF type RGCs. Perhaps one of the most intriguing outcomes of this study, also consistent with observations of perception (Idrees et al., 2020), is that the suppressive effects observed in RGCs are not exclusively triggered by saccades, but occur for many scenarios involving sequential visual stimulation, which are ever-present during natural vision. Therefore, while the results described here are crucial for understanding the mechanisms of saccadic suppression, they also elucidate more general mechanisms of retinal signal processing across any time-varying visual input over short time scales (10 ms to 1 s).

Results

Experimental Approach

We measured the modulation of retinal ganglion cell (RGC) output following saccade-like changes of the visual input with a variety of different light stimulation strategies (Fig. S1). The basic experimental paradigm was similar to that described in (Idrees et al., 2020). Briefly, we recorded spiking activity of RGCs in isolated ex vivo mouse retinae using both high-density and low-density multi-electrode arrays (MEAs). Each retina was exposed to a background texture having one of several possible spatial scales that defined its spatial spectrum ("fine" to "coarse", Methods, Fig. S2). We simulated saccade-like image displacements by rapidly translating the texture globally across the retina (Methods; Fig. 1a). Most RGCs responded robustly to such saccade-like texture displacements (see Fig. 1b for responses of example ON and OFF RGCs). At different times relative to the saccade-like texture displacements ("saccades" from now on), we presented a brief probe flash (Fig. 1c). We then

134 analyzed how the response (spike rate of the RGC) to this probe flash was influenced
135 by the preceding saccade, by comparing it to the response to the flash presented in
136 isolation (baseline). To quantify RGC response modulation, we calculated a
137 modulation index (Methods) as follows: we first isolated the flash-induced response
138 component by subtracting the saccade-only response (e.g., Fig. 1b) from the response
139 to the composite saccade-flash stimulus (e.g., Fig. 1c). Based on this flash-induced
140 response component (Fig. 1d), we calculated the modulation index as $(r_d - r_b)/(r_d + r_b)$.
141 Here, r_d is the peak response to the probe flash presented with a delay d relative to
142 saccade onset, and r_b is the baseline (peak response to the flash presented ~2 s after
143 the saccade). This modulation index is negative when flash-induced responses are
144 suppressed (Fig. 1d shows, on the horizontal dashed line, the modulation index for the
145 responses at each flash-time). In yet further recordings we applied various
146 manipulations to this base paradigm to probe for the mechanisms underlying
147 modulation of RGC responses following saccades. To generalize our findings across
148 other species, we also performed similar analyses of pig and macaque RGC data.

149 **Similarities and differences in retinal saccadic suppression across ON and OFF**
150 **type RGCs**

151 Suppression was robust across most RGCs that we recorded from, consistent with
152 what we reported previously (Idrees et al., 2020). Here, we more closely inspected
153 functionally different RGCs. Specifically, throughout this study, we divided RGCs into
154 ON and OFF types, i.e. into RGCs responding best to light increments or decrements,
155 respectively (Methods). We always quantified the modulation index defined above for
156 ON RGCs based on their responses to bright probe flashes and for OFF RGCs based
157 on their responses to dark probe flashes (Fig. 1c, d). Flash responses following a
158 saccade were suppressed in both ON and OFF RGCs, as seen in Fig. 1d for example
159 cells. Fig. 1e shows the temporal profile of the mean population modulation index, and
160 Fig. S3 the underlying population data. Suppression was consistently stronger for
161 coarser background textures (Figs. 1e, S3), for both ON and OFF RGCs. This is
162 consistent with (Idrees et al., 2020), where we showed that this dependency on the
163 texture can be explained by the distinct statistics of luminance and contrast changes
164 when coarse or fine textures move across the RGCs' receptive fields. However, a
165 striking difference existed in suppression recovery times: OFF RGCs recovered by

166 ~350 ms after saccade onset, whereas ON RGCs recovered only by ~1 s. Similar
167 results were obtained under scotopic conditions for coarse textures, while suppression
168 for fine textures was very weak (Fig. S4; all other mouse retina data was recorded at
169 mesopic conditions). In general, the presence of post-saccadic suppression of probe
170 flash responses in both ON and OFF type RGCs suggests a common mechanistic
171 theme across these cell types (Idrees et al., 2020). On the other hand, the different
172 recovery times indicate either additional suppressive mechanisms in ON RGCs or
173 additional recovery mechanisms in OFF RGCs.

174 **Spatial origin of retinal saccadic suppression**

175 ***Global component of suppression***

176 To probe the mechanisms underlying suppression and its differences across ON and
177 OFF type RGCs, we first examined the spatial origin of suppression. We hypothesized
178 that suppression of flash responses was caused by circuits detecting rapid global shifts
179 across the retina. Typically, these circuits include a lateral network of interneurons,
180 communicating with RGCs even from beyond their classical center-surround receptive
181 field (i.e., from their periphery, or far surround) (Lin and Masland, 2006; Roska and
182 Werblin, 2003). To test whether suppression was caused by such circuits, we modified
183 the spatial layout of the paradigm: we placed a square mask of 1000 x 1000 μm^2
184 (Fig. 2a, right) to restrict the saccades to the periphery of an RGC's receptive field.
185 Similar to the previous experiments, the probe flash was either a dark or bright flash
186 presented over the entire retina, including the masked region. Figure 2b shows the
187 mean population modulation indices of ON RGCs (top) and OFF RGCs (bottom) from
188 these experiments (Fig. S5 depicts the underlying population data and shows
189 responses of representative ON and OFF RGCs from these experiments). In OFF
190 RGCs, responses to full-field probe flashes were no longer suppressed when
191 saccades were restricted to the periphery. The responses of ON RGCs, on the other
192 hand, were still suppressed in this condition. The resulting suppression was however
193 weaker and shorter-lived (recovered by 350 ms) than with full-field saccades. These
194 observations (Figs. 2b, S5c) were robust across ON and OFF RGCs whose receptive
195 fields were completely contained within the mask (Fig. S5b).

196 We will refer to this component of suppression in ON RGCs, which originates from the
197 periphery, as the “global component” from now on. Such spatially far-reaching
198 inhibition is often mediated through GABAergic wide-field amacrine cells. We tested
199 this hypothesis by blocking $GABA_A$ receptors. Indeed, in the periphery saccade
200 condition, the modulation index for most ON RGCs was around 0 in the presence of
201 the $GABA_A$ receptor antagonist SR-95531 (Fig. 2b, S5d). These results suggest that
202 this short-lived global component of suppression is caused by inhibition via GABAergic
203 amacrine cells, perhaps similar to the polyaxonal amacrine cells described previously
204 (Baccus et al., 2008; Ölveczky et al., 2003; Roska and Werblin, 2003). Thus, while
205 suppression is indeed partially caused by circuits detecting global changes across the
206 retina, those circuits seem to act predominantly on ON RGCs, and even there, they
207 only account for a fraction of the total suppression observed with full-field saccades
208 (without mask), which lasts longer. Other, probably more local sources of suppression
209 must exist that account for most of the suppression in ON RGCs and all of the
210 suppression in OFF RGCs.

211 ***Local components of suppression***

212 To understand the more local components of suppression, we used different analyses
213 and manipulations of the main experimental paradigm. As we will see below, the more
214 local components can be subdivided into a “central” and a “surround” component.
215 First, we eliminated the global component, by repeating our normal full-field saccade
216 paradigm in the presence of GABA receptor blockers. The suppression profile of both
217 ON and OFF RGCs was only weakly affected upon blocking $GABA_{A,C}$ receptors (5 μM
218 SR-95531 and 100 μM Picrotoxin; Fig. 2c, S6a). Since the GABA-block eliminates the
219 global component of suppression, the remaining more local components did not seem
220 to rely on GABAergic inhibition. Also, this suggests that the local components
221 dominate retinal saccadic suppression under full-field conditions. We then also
222 blocked glycine receptors (1 μM of Strychnine; Fig. 2d, S6b) to test if the local
223 components of suppression were caused by local inhibition via glycinergic pathways.
224 Here again, the suppression profiles of both ON and OFF RGCs were only weakly
225 affected upon blocking glycine receptors in combination with blocking $GABA_{A,C}$
226 receptors. Therefore, inhibitory synaptic interactions are not the major mechanism
227 behind the local components, which dominate suppression of RGCs.

228 Next, we tested whether these local components originated from within the receptive
229 field center. For this, we modified the spatial layout of our paradigm to exclude
230 saccades from the very center of the receptive field. Simply reducing the size of our
231 mask would have severely decreased the number of simultaneously recorded cells
232 located inside the mask, and we therefore resorted to a different strategy: saccades
233 and flashes were presented in small square regions spread across the retina,
234 separated by gaps kept at mean luminance ("checkerboard mask", Fig. 2e). In one
235 condition (Fig. 2e, left), we presented saccades and flashes in all regions of the
236 checkerboard mask; in the other condition (Fig. 2e, right), saccades and flashes were
237 presented in alternate regions. With this second arrangement, saccades were
238 excluded from at most ~300 x 300 μm^2 of a cell's receptive field center, even if that
239 cell was perfectly centered on a non-saccade region. Flashes were presented in the
240 set of regions that included the square region covering the receptive field center of the
241 analyzed RGC (Fig. S7a).

242 Probe flash responses following saccades were suppressed in both ON and OFF
243 RGCs when the saccade and flash were presented in all regions (Fig. 2f, thick lines;
244 Fig. S7c; see Fig. S7b for example cells), consistent with the suppression observed
245 after full-field saccades (Figs. 1, S3). When saccades were excluded from the
246 receptive field center, and were presented in alternate regions to the flash, the flash
247 responses were no longer suppressed in OFF RGCs (Fig. 2f, bottom, thin line), even
248 though these cells showed spiking responses to saccades themselves (Fig. S7b). In
249 fact, flash responses were even enhanced. This suggests that the local component of
250 suppression in OFF RGCs arises fully from within the receptive field center ("central
251 component"). This highly localized origin of suppression in OFF RGCs was further
252 confirmed by additional analysis of the large mask experiments (see Figs. S7d, e). In
253 ON RGCs, on the other hand, suppression persisted (Fig. 2f, top; Fig. S7c), even
254 though a loss in suppression was apparent for flashes presented immediately after the
255 saccade, at 117 and 150 ms (marked with an arrow in Fig. 2f). This suggests that in
256 ON RGCs, part of the early suppression originates from the "central component". The
257 leftover suppression during these early time points might be explained by the global
258 component of suppression, described above (Fig. 2b, S5c), which should also be
259 triggered under this experimental setting. However, since the global component also

recovers quickly (by 350 ms, Fig. 2b, S5c), the persisting suppression at the later time points (350 ms and beyond) needs to originate from yet another source beyond the receptive field center. We call this the “surround component”, and it may originate from the ON RGCs’ immediate surround, which also experiences the saccade under this experimental setting. Therefore, in ON RGCs, the local component of suppression can be divided into a central and a surround spatial component.

Summary of retinal saccadic suppression spatial origins

In summary, our data suggests that retinal saccadic suppression is mediated by at least three components with distinct spatial origins and temporal properties (Fig. 3): a central, surround, and global component. Suppression in OFF RGCs is mediated exclusively by the central component, which originates from the cell’s receptive field center and is characterized by fast onset and fast recovery (by 350 ms after saccade onset). In ON RGCs, we most directly observed the global component (Figs. 2b, S5a). It extends into the periphery and its timing is similar to the central component in OFF RGCs. Only this global component is affected by blocking GABA receptors (Figs. 2b, S5b). During full-field saccades, removing this component by blocking GABA receptors has little effect on the overall suppression (Figs. 2c, 2d, S7), suggesting a more dominant role of the remaining components. The central component in ON RGCs can only be observed by the loss in suppression for early flashes when saccades are excluded from the receptive field center (marked with an arrow in Fig. 2f, top). Its full duration and time course are obscured by the concurrently acting global and surround components. However, given the identical pharmacological dependencies and spatial origins, it is plausible that the central component is symmetric across ON and OFF RGCs with a common underlying mechanism. Therefore, the longer suppression in ON RGCs can neither be attributed to the central nor global components. It likely originates from the immediate surround of the receptive field. This surround component is long lasting (recovers by ~1s) and has a slow onset (Figs. 2f, S3).

Suppression is triggered by interaction between consecutive stimuli of opposite polarity

We previously showed (Idrees et al., 2020) that retinal and perceptual saccadic suppression not only occur after texture displacements, but also after instantaneous

texture jumps and structure-free uniform luminance steps. These observations suggested that saccadic suppression is the consequence of rather general mechanisms in which the response to a second stimulus (here: probe flash) gets suppressed by a previous visual transient (caused by saccades or luminance steps). In the following, we apply additional analysis to the luminance-step paradigm (Fig. S1b) dataset of (Idrees et al., 2020), to investigate how the polarity and strength of the visual transients affect the suppression of ON and OFF RGCs.

Similar to all previous experiments, we analyzed the modulation index of ON and OFF RGCs separately, using bright probe flashes to analyze ON RGCs and dark probe flashes for OFF RGCs. Consistent with the suppression after texture displacements (Figs. 1e, S3), responses to flashes after luminance steps were strongly suppressed in both ON and OFF RGCs, and ON RGC suppression outlasted suppression in OFF RGCs (Fig. 4a, S8a). The two seemingly different experimental paradigms may therefore trigger similar mechanisms in the retina.

We hypothesized that the response to a luminance step might strongly activate RGCs, so that the response to a subsequent probe flash would drive the cells into adaptation or saturation, effectively resulting in suppressed flash responses. At least for the local components of suppression, this could be a viable mechanism as suppression is not caused by inhibitory synaptic interactions. If this was indeed the case, then positive-contrast luminance steps would suppress responses to bright flashes in ON RGCs, and negative-contrast luminance steps would suppress responses to dark flashes in OFF RGCs. To test this, we separately analyzed the effects of positive- and negative-contrast luminance steps on probe flash responses (Fig. 4b). Surprisingly, the resulting effects were contrary to our adaptation/saturation hypothesis: the responses of ON RGCs to bright probe flashes were only weakly suppressed after positive-contrast luminance steps (Fig. 4b, left), but strongly suppressed following negative-contrast luminance steps (Fig. 4b, right). Similarly, responses of OFF RGCs to dark probe flashes were weakly suppressed by negative-contrast luminance steps (Fig. 4b, right), but strongly suppressed by positive-contrast luminance steps (Fig. 4b, left). Fig. S8 shows the underlying population data for these experiments, and Figs. S9a, b show the spiking response of a representative ON and OFF RGC, respectively. While ON RGCs did show a small component of suppression in support

323 of our adaptation/saturation hypothesis (Fig. 4b left panel, see Fig. S9a left column
324 and Fig. S10a for a detailed analysis), the dominant suppressive effect in both ON and
325 OFF RGCs was caused by luminance steps with the opposite contrast as the
326 subsequent flash.

327 Such crossover style of suppression would be consistent with mechanisms involving
328 crossover inhibition via amacrine cells (Werblin, 2010), where activation of OFF
329 pathways (here: by the negative-contrast luminance step) would inhibit responses in
330 the ON pathway (here: to the bright probe flash) and vice versa. However, consistent
331 with our earlier experiments (Fig. 2c, d), suppression in ON RGCs still persisted upon
332 blocking $GABA_{A,C}$ and glycine receptors (5 μM SR-95531, 100 μM Picrotoxin and 1 μM
333 Strychnine) (Fig. 4c). We could not calculate a modulation index for OFF RGCs under
334 these conditions because they did not respond to brief probe flashes in the presence
335 of the pharmacological agents, and therefore the modulation index was
336 mathematically undefined. However, in our texture displacement experiments, the
337 same pharmacological agents (Fig. 2d) had no substantial effect on OFF RGC
338 suppression. The crossover-style suppression observed in Fig. 4b was therefore
339 unlikely to be caused by classical crossover inhibition pathways involving amacrine
340 cells and $GABA_{A,C}$ or glycine receptors.

341 **Central component of suppression results from cone response kinetics and**
342 **nonlinearities in downstream retinal pathways**

343 So far, our experiments suggest that suppression in OFF RGCs (1) is mediated solely
344 by the central component of suppression that originates in the receptive field center
345 (Figs. 2e, S7b-e), (2) is predominantly triggered by the interaction between
346 consecutive stimuli with opposite polarity (Figs. 4b, S8b), and (3) is not caused by
347 inhibitory amacrine cells (Figs. 2c, 2d, S6). Similar conclusions can be drawn for the
348 central component of suppression in ON RGCs. Together, these results restrict the
349 possible cellular substrates for this central suppressive mechanism to the feed-forward
350 pathway in the retina, namely photoreceptors - bipolar cells - RGCs. We wondered
351 whether opposite-polarity stimulus-stimulus interactions could already modulate the
352 responses of photoreceptors themselves. For this, we recorded the output of cones
353 with an intensity-based glutamate-sensitive fluorescent reporter (iGluSnFR) (Marvin

354 et al., 2013; Szatko et al., 2020), predominantly expressed in horizontal cells
355 postsynaptic to cone terminals (Methods). We presented a shortened version of the
356 luminance step paradigm in which a homogeneous background alternated between a
357 brighter and darker gray value (Fig. S1c) to induce positive-contrast (+0.4 Michelson
358 contrast) and negative-contrast (-0.4 Michelson contrast) luminance steps. Dark or
359 bright probe flashes (100 ms duration, -0.33 or +0.33 Michelson contrast, respectively)
360 followed the luminance steps at different delays (50, 250, and 2000 ms), with the flash
361 at 2000 ms serving as baseline.

362 The luminance steps caused sustained changes in the cones' glutamate output
363 (Fig. 5a). The transient responses to the probe flashes were superimposed on these
364 glutamate modulations (Fig. 5b). This superposition was mostly linear and did not
365 indicate nonlinear effects such as adaptation or saturation. Therefore, when we
366 isolated the flash responses by subtracting the step responses, the resulting peak
367 flash responses were only weakly affected by the preceding luminance step (Fig. 5c).
368 Thus, at the level of the cone output (Fig. 5b), there was hardly any suppression when
369 only considering the peak of the probe flash responses (Fig. 5c). How does the
370 suppression observed at the level of RGC output arise from effectively linear cone
371 responses? The answer lies in other properties of the cone response, such as its
372 kinetics, which will be captured by downstream retinal pathways.

373 To demonstrate this, we used a previously published phenomenological model of
374 retinal processing. In the model (Drinnenberg et al., 2018), RGC responses are
375 described by passing a "light stimulus" to model photoreceptors, feeding their output
376 through a set of linear-nonlinear filters to describe the processing in different bipolar
377 pathways (Methods), and eventually converting these filter outputs into RGC spiking.
378 Here, as the first step of analysis, we fitted the parameters of the model cone to reflect
379 our measured data of cone output. The model faithfully explained the observed cone
380 responses (Fig. S11) and gave us the opportunity to calculate cone responses to
381 flashes presented at additional time points. This modeled cone output to step-flash
382 combinations was fed into the model bipolar cells, finally yielding model RGC
383 responses (Fig. 6). In the model, different RGC types can be described by varying the
384 bipolar cell filter properties. We first investigated transient RGC responses (Fig 6a-c)
385 and calculated a modulation index (Fig. 6d) comparable with the modulation index of

386 our real RGC data. As a control, we also passed the raw cone output data, instead of
387 the fitted cone model, to the model bipolar cells and found qualitatively the same
388 results (Fig. S12).

389 The model's ON and OFF RGCs (Fig. 6d) showed crossover-style suppression that
390 was consistent with the suppression of real RGCs under similar luminance step
391 experiments (Fig. 4b): the model's ON RGC showed strong suppression to the bright
392 flashes presented immediately after the negative-contrast luminance step (Fig. 6d,
393 right), while flashes after the positive-contrast luminance step were only weakly
394 affected (Fig. 6d, left). Suppression recovered by 200 ms, consistent with the recovery
395 time for the central component of suppression in real RGCs. Similarly, the model's
396 OFF RGC showed strong suppression of its response to dark flashes presented
397 immediately after the positive-contrast luminance step (Fig. 6d, left); suppression was
398 absent in OFF RGC when the dark flash was presented later or after a
399 negative-contrast luminance step (Fig. 6d). The markers on the curves in Fig. 6d
400 correspond to the time points when the flashes were presented to the cones in the
401 experiments depicted in Fig. 5. Model RGC responses to step-flash combinations and
402 flash-induced responses at these time points are shown in Fig. 6a-c.

403 What mechanism within the model led to the emergence of the suppressive effect in
404 RGC responses, despite the mostly linear response superposition at the cone
405 output? In the model, the bipolar cells have transient filter properties and are driven
406 predominantly by the instantaneous rate of change in the cone output, i.e. its
407 derivative, rather than by the absolute cone output. The response to a probe flash
408 presented immediately after an opposite-contrast luminance step (50 ms) occurred
409 during the initial phase (ramp) of the cone response to the luminance step (Fig. 5b,
410 columns 2 and 3). This causes a much smaller rate of change in cone output and
411 therefore drives the downstream bipolar cells only weakly, resulting in weak or even
412 completely suppressed model RGC responses (Fig. 6c, columns 2 and 3). On the
413 other hand, flashes presented during the steady state phase of the luminance step
414 response (250 ms and 2000 ms in Fig. 5b, columns 2 and 3), or flashes presented
415 immediately after (50 ms) a same-contrast luminance step (Fig. 5b, columns 1 and 4)
416 caused larger instantaneous changes in the cone output, and therefore resulted in

417 relatively stronger spiking (250 ms and 2000 ms in Fig. 6c; 50 ms in Fig. 6c, columns
418 1 and 4).

419 If suppression observed at RGC output did indeed result from the weaker rate of
420 change in the cone output, less transient RGCs should show weaker suppression
421 because they reflect the absolute cone output signal more faithfully. To test this, we
422 varied the linear-nonlinear filter of the model bipolar cell to make the retinal pathway
423 less transient (Methods). Indeed, the resulting crossover-style suppression was
424 weaker in model RGCs with less transient response properties, indicated by the
425 negative modulation index slope in Fig. 6e; seen in the ON RGC suppression after
426 negative-contrast steps (blue lines in row 2) and OFF RGC suppression after
427 positive-contrast steps (red lines in row 1); columns represent different time points
428 sampled. Curious if this effect was also present in our real RGC data, we re-analyzed
429 the data of Fig. 4 and evaluated suppression as a function of RGC transiency
430 (Methods). The result was congruent with the model prediction: suppression was
431 weaker in less transient (more sustained) cells (Fig. 6f).

432 The analyses above suggest that the central component of retinal saccadic
433 suppression does not have a single site of origin. Instead, it appears to emerge from
434 the relatively slow kinetics of cone responses (such that flash responses ride on the
435 initial rising/falling phase of the cone's step response), combined with temporal
436 properties and nonlinearities of downstream retinal pathways. The downstream
437 pathways shape the exact strength and time course of RGC suppression. We term
438 this novel retinal processing motif "dynamic reversal suppression": "dynamic" because
439 of the necessarily tight temporal link between responses to the two consecutive stimuli;
440 and "reversal" because the response to an event gets suppressed when it reverses
441 the cone output triggered by the first stimulus.

442 **Generalization to other species**

443 Retinal saccadic suppression, at least its central component, was triggered by
444 stimulus-stimulus interactions (Figs. 4, 6, S8), governed by general retinal signal
445 processing, without the need for any specialized "saccadic suppression" circuit. It is
446 likely that such general processing is conserved across species. Indeed, we observed

447 quantitatively similar retinal saccadic suppression in pig ON and OFF RGCs
448 (Fig. S13), including the dependency on background texture statistics. Interestingly,
449 like in mouse, OFF RGCs in pig retina also recovered faster than ON RGCs,
450 suggesting that the surround component of suppression was also present in pig ON
451 RGCs. In an additional experiment, we also recorded the activity of RGCs from an ex
452 vivo macaque retina while subjecting it to a shorter version of the luminance step
453 paradigm (Fig. S1b) with fewer conditions than in the original paradigm. Our results
454 (Fig. 7) indicate that macaque RGC responses to probe flashes, following luminance
455 steps, are suppressed in a way similar to mouse retina. However, more data will be
456 required to determine the population trend and for characterizing the dictionary of
457 response modulations in macaque retina.

458 **Downstream visual areas may modulate retinal saccadic suppression**

459 Given the similarities we previously described between retinal and perceptual saccadic
460 suppression (Idrees et al., 2020), it was tempting to test whether the crossover style
461 of suppression, observed in the retina (Fig. 4b), was also reflected in perception. We
462 therefore conducted human psychophysics experiments where we asked human
463 subjects (N = 5) to maintain saccade-free fixation, while we simply changed the
464 luminance of the homogenous background to a brighter (0.3 to 0.56 Michelson
465 contrast) or darker (-0.3 to -0.56 Michelson contrast) background (Fig. 8a; Methods).
466 At random times relative to the luminance step, we presented a dark (-0.033 Michelson
467 contrast) or bright probe flash (+0.033 Michelson contrast), at one of four locations in
468 the subjects' field of view. At trial end, the subjects were asked to localize the probe
469 flash.

470 Irrespective of the step → flash combination, subjects were strongly impaired in their
471 ability to localize the probe flashes presented around the time of the luminance step
472 (Fig. 8b). Most interesting in this context was the combination of negative-contrast
473 luminance steps with dark probe flashes. In mouse retina, even though few OFF RGCs
474 did show weak suppression to this combination (Fig. S8b, inverted histograms in row
475 2), this effect was virtually absent at the population level (Fig. 4b, right panel). In
476 human perception, however, this combination led to strong suppression (Fig. 8b, right
477 panel). We cannot exclude that stronger retinal suppression to this specific

478 combination might be present under different light or stimulus conditions. Another
479 possibility is that it might be more pronounced in the retina of humans and other
480 primate species (Fig. 7). Nonetheless, visual mechanisms of suppression certainly
481 exist in higher visual brain areas (Idrees et al., 2020). Perceptual suppression after
482 same-contrast stimulus combinations may arise from processing in these higher visual
483 brain areas, which may modulate and complement retinal saccadic suppression to
484 achieve robust effects at the perceptual level.

485 Discussion

486 For most RGCs that we recorded, responses to brief probe flashes were strongly
487 suppressed when presented after saccade-like texture displacements across the
488 retina. In fact, similar suppression occurred when texture displacements were replaced
489 by sudden uniform changes in background luminance, suggesting that suppression
490 was caused by rather generic mechanisms, triggered by visual transients across the
491 retina, rather than specialized suppression circuits that react to image motion. We
492 found that the suppression strength depended on four main factors: (1) strength of the
493 visual transients, governed by the statistics of the background texture or the contrast
494 of the luminance step; (2) elapsed time following the visual transient; (3) RGC polarity
495 (ON vs. OFF RGCs); and (4) RGC response properties (RGC transiency). Stronger
496 visual changes, elicited either by coarser textures or larger luminance step contrasts,
497 caused stronger suppression, peaking approximately 50 ms after the stimulus offset
498 (Figs. 1e, 4). The recovery times depended on RGC polarity: OFF RGCs recovered
499 by 250 - 350 ms whereas suppression in ON RGCs lasted for up to 1 s (Figs. 1e, 4).
500 The suppression was stronger in more transient RGCs (Fig. 6e, f). We identified at
501 least three components of retinal saccadic suppression, with distinct spatial origins,
502 defined as central, surround, and global components (Fig. 3). These components were
503 mediated by different underlying mechanisms.

504 The central component was the only source of suppression in OFF RGCs, and the
505 dominant source in ON RGCs for time points immediately after a full-field saccade or
506 luminance step. This component was short-lived (~250-350 ms) and originated from a
507 cell's receptive field center. It was triggered by opposite-polarity stimulus-stimulus
508 interactions, which naturally occur during saccades and other forms of sequential

509 visual stimulation. The relatively slow temporal dynamics of the cone photoreceptor
510 responses to two opposite-polarity consecutive stimuli were the basis for subsequent
511 non-linear processing, ultimately suppressing RGC response to the second stimulus.
512 Therefore, the central component of suppression cannot be pinpointed to one specific
513 site but seems to be an emergent property. We call this novel processing motif
514 "dynamic reversal suppression". Such a mechanism, where the cone response itself
515 remains linear, but nonetheless forms the basis for subsequent nonlinear response
516 modulation, is clearly different from adaptation (Clark et al., 2013) or desensitization
517 (Baylor and Hodgkin, 1974) mechanisms within the cones, which would evoke
518 nonlinear responses of the cones themselves.

519 The suppressive mechanism of the central component also suggests that perceptual
520 saccadic suppression is derived, at least in part, from the inherent response properties
521 of photoreceptors, the very first cell in the visual processing cascade. In fact, this early
522 implementation could also explain why we observed suppression in most RGCs we
523 recorded from (Figs. S3, S8, S13), covering a wide spectrum of response properties
524 and therefore presumably many RGC cell types (see Supplementary Fig. 6 of Idrees
525 et al., 2020). Still, our results suggest that the suppression initiated at the level of cone
526 photoreceptors is translated differently by the different parallel pathways in the retina,
527 leading to variability in response suppression at the ganglion cell level (such as the
528 stronger suppression in more transient RGCs, Fig. 6e, f). Further cell type
529 classification will be required to relate the degree of modulation with pathway
530 specificity. The type and degree of modulation might also differ across species, even
531 though we see qualitatively similar suppression in mouse, pig, and macaque RGCs.

532 ON RGC sensitivity, in addition to this central component, is suppressed by two more
533 components. First, the global component is a fast but short-lived (~250-350 ms)
534 component, caused by inhibition via GABAergic wide field amacrine cells, triggered by
535 global image changes and carried to the RGC from as far as the cell's periphery
536 (Figs. 2b, S5). This likely belongs to the same class of circuits that suppresses RGC
537 responses to global motion (Baccus et al., 2008; Roska and Werblin, 2003). These
538 circuits were previously suggested to suppress motion awareness during saccades, a
539 phenomenon known as saccadic omission. As indicated by our results, such circuits
540 also contribute towards suppressing RGC sensitivity even after the motion is

541 completed (i.e. saccadic suppression). However, since their influence is masked by
542 more local components of suppression during full-field saccades (Fig. 2c, 2d, S6), they
543 are unlikely to account for perceptual saccadic suppression. The global suppressive
544 component mediated by GABAergic inhibition is nevertheless a mechanism to
545 process global visual changes, in addition to the several others (Wei, 2018). It may,
546 for example, play a role in perceptual modulations during smooth pursuit eye
547 movements (Schütz et al., 2011). Here, the central component of suppression will not
548 be triggered in RGCs whose receptive field centers are locked to the tracked object;
549 but these RGCs will still be suppressed by the global component.

550 The second additional component is the surround component. It seems to act with a
551 delay of ~200 ms and can last for up to 1000 ms. The spatial origins of this component
552 are not very well understood, but our data indicate that it presumably arises from the
553 immediate surround of a cell's receptive field. Additionally, similar to the central
554 component, it does not rely on $GABA_{A,C}$ or glycine receptors (Fig. 2c, 2d, S6), but the
555 exact mechanisms remain to be explored. Possible mechanisms could involve
556 negative feedback of horizontal cells onto the cones (Drinnenberg et al., 2018;
557 Kemmler et al., 2014). This slower component most likely contributes to the longer
558 recovery times observed in ON cells. Interestingly, visual masking in cat LGN also
559 lasts longer in ON versus OFF cells (Schiller, 1968), which may be a consequence of
560 the effects we describe here in the retina. While this surround component plays an
561 important role in shaping RGC and downstream neural responses following a visual
562 transient, its contribution to perceptual saccadic suppression can also be disputed.
563 This is because, during real saccades, eye-movement related signals (e.g., corollary
564 discharge) shorten the duration of suppression caused by visual mechanisms (Idrees
565 et al., 2020), such that the long-lasting surround component may not critically shape
566 perception. Yet another additional component of suppression, based on saturation-like
567 mechanisms (Fig. 4b left, S10a), was found only in ON RGCs. It is possible that this
568 component originates at the level of bipolar cells, especially because response
569 saturation has been observed predominantly in ON bipolar cells but not in OFF bipolar
570 cells (Schreyer and Gollisch, 2020). In summary, while Fig. 3 summarizes the three
571 spatial components of suppression and their temporal properties, these components
572 in turn can have further sub-components.

Irrespective of which components of retinal saccadic suppression contribute towards perceptual saccadic suppression, our results show that retinal responses to stimuli following visual transients are modulated concurrently by several mechanisms (Fig. 3). Additional mechanisms might exist under different stimulus conditions. From the perspective of retinal visual feature processing, this would be consistent with how multiple mechanisms concurrently process other visual features in the retina, such as motion (Wei, 2018). The retinal suppression that we studied likely contributes to several other visual phenomena, such as visual masking (Breitmeyer, 2007) or neural adaptation with successive stimuli (Mayo and Sommer, 2008). The similarities between the observations there and the suppression that we observed in the retina suggest that the retina may be a common neural substrate for these seemingly different types of perceptual phenomena, unifying their underlying mechanisms. The retinal processing described here may also contribute towards specialized visual-motor tasks. For example, while threading a needle, microsaccades will jitter the needle and its background across the retina. RGCs exposed to the background will experience stronger visual transients than RGCs exposed to the needle. As a result, RGCs 'seeing' the background might show suppressed responses following microsaccades, perceptually blurring out the background. This relative enhancement of the fixated object by background suppression could be valuable for visual tasks such as object recognition.

It is remarkable that an elementary property of retinal suppression, i.e. its dependence on the scene statistics (Fig. 1e), is clearly preserved all the way to perception (Idrees et al., 2020). However, retinal suppression alone cannot explain all perceptual effects of saccadic suppression. For example, suppression before a saccade (or a luminance step) is observed perceptually (even in the absence of eye movements, Fig. 8), but not in the retinal output (Idrees et al., 2020). Similarly, not all properties of retinal suppression were preserved in perception. The crossover style of suppression observed in the retinal output of mice (Fig. 4b) was not observed perceptually in humans (Fig. 8). The more far-reaching perceptual suppression may be the result of additional processing beyond the retina (Shapley and Enroth-Cugell, 1984). Alternatively, our results may not capture the full array of retinal processing. For one, our stimulus conditions in mouse retina experiments may not have been

comprehensive enough to capture all retinal suppressive effects. Further, the retinal output of humans and other primate species (Fig. 7) might differ from mouse retina in this respect.

Retinal suppression is only one way that the retina alters its output during dynamic vision. Other forms certainly co-exist, such as brief changes in RGC polarity following peripheral shifts (Geffen et al., 2007) or sensitization of some RGC types following a change in background luminance (Appleby and Manookin, 2019). These and several other studies (Amthor et al., 2005; Barlow et al., 1977; Enroth-Cugell and Jakiela, 1980; Krishnamoorthy et al., 2017; Noda and Adey, 1974; Passaglia et al., 2009; Roska and Werblin, 2003), together with ours, demonstrate the complex image processing capabilities in the retina to facilitate downstream visual processing for the ultimate service of perception during natural vision. Looking forward, the detailed characterization of retinal output provided here paves the way to investigate the visual features that the retina encodes during dynamic vision. Moreover, it also paves the way to investigate the interactions between retinal and extra-retinal (visual and non-visual) mechanisms of saccadic suppression, to further our understanding of how the visual system maintains stability in the face of constant disruptions.

Acknowledgements

We thank Elisabeth Gustafsson for providing technical support; Andreas Hierlemann for providing the HiDens CMOS MEA system and helping establish our high-density MEA recordings; Roland Diggelmann for helping in setting up the pipeline (including providing code) for automatic spike sorting of high-density MEA recordings; Martin Schenk at the Department of Experimental Surgery, Tübingen, for providing us domestic pig eyes. Our work was supported by funds of the Deutsche Forschungsgemeinschaft (DFG) to the Werner Reichardt Center for Integrative Neuroscience (EXC 307) and to TAM (MU3792/1-1 and MU3792/3-1). TAM received support from the Tistou and Charlotte Kerstan Foundation. SI, TAM and ZMH were also supported by an intra-mural funding program (Project 2013-05) of the Werner Reichardt Center for Integrative Neuroscience. FF was supported by a Swiss National Science Foundation Ambizione grant (PZ00P3_167989) and Swiss National Science Foundation Eccellenza grant (PCEFP3_187001). MPB and ZMH were further funded

by the SFB 1233 on “Robust Vision” (DFG, project number 276693517). KF was supported by the Bundesministerium für Bildung und Forschung (BMBF, 01GQ1002) and the Max Planck Gesellschaft (MPG, M.FE.A.KYBE0004).

Author contributions

TAM conceptualized the study; SI and TAM designed the overall study; FF developed and supervised computational modeling; SI, MPB, AK, KF, ZMH, FF and TAM designed experiments; SI performed ex vivo mouse and pig retina experiments; AK performed ex vivo macaque retina experiment; MPB performed human psychophysics experiments; KF performed viral injections; MK performed cone imaging experiments; SI and FF implemented computational model; All authors analyzed and interpreted the data and wrote the manuscript.

Declaration of interests

The authors declare no competing interests.

Data availability

All data presented in this paper are stored and archived on secure institute computers and are available upon reasonable request.

Code availability

All code used for analysis and computational modeling is available upon reasonable request.

Figures

Figure 1

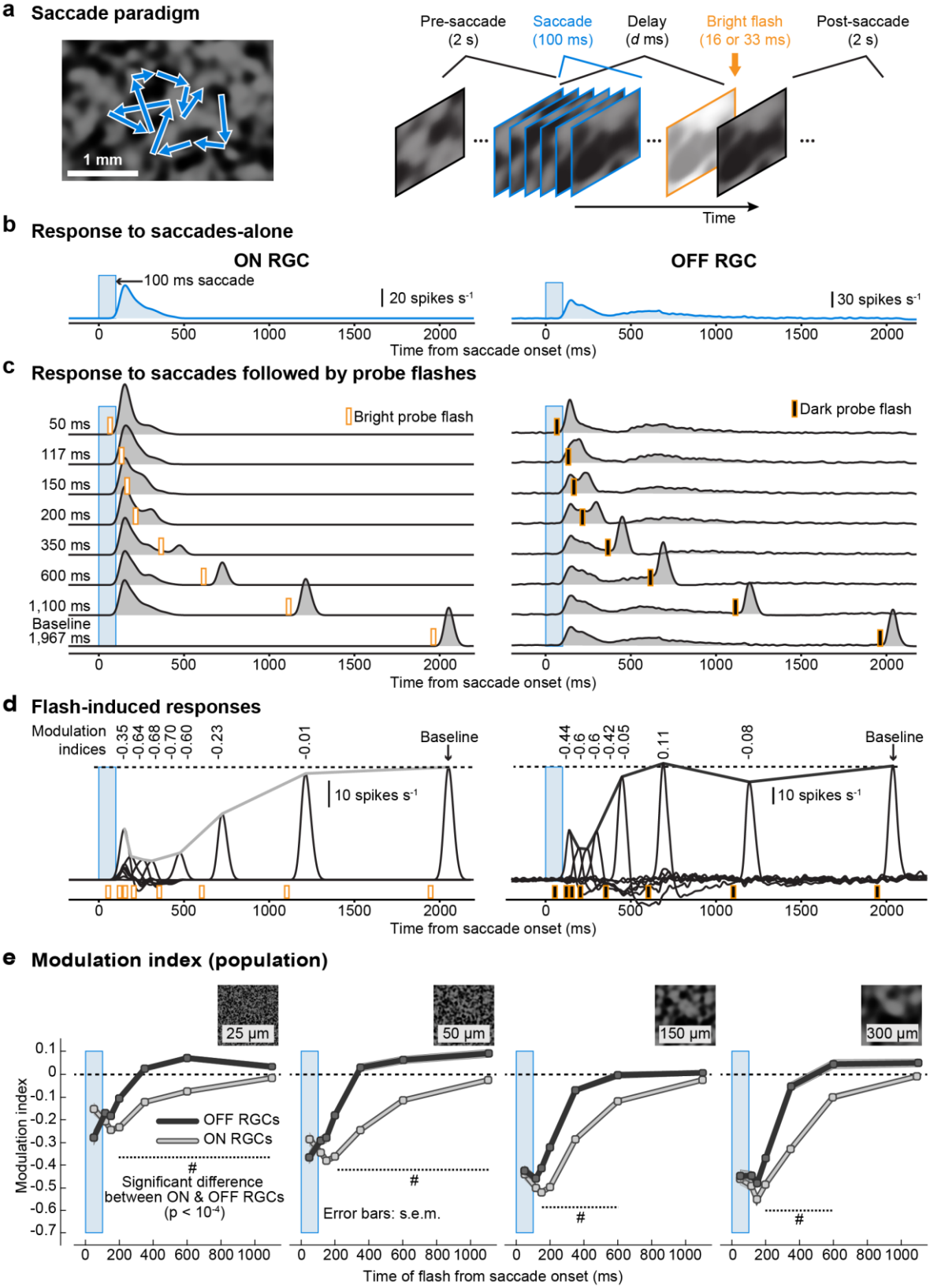

Figure 1 Similarities and differences in retinal saccadic suppression across ON and OFF RGCs.

a. RGC action potentials were recorded from ex vivo retinae placed on multielectrode arrays. Saccades were mimicked by displacing a texture projected onto the retina (blue arrows in left panel indicate texture displacement paths). The texture remained static for 2 s and was then displaced over 100 ms (blue outlines) followed by a brief probe flash (here bright probe flash is depicted, orange outline). Each trial consisted of 39 such successive saccade-flash sequences (Fig. S1a).

b,c. Average activity (firing rate) of an example ON RGC (left column) and OFF RGC (right column) to 39 saccade sequences not followed by a probe flash (**b**), and to 39 saccade sequences followed by probe flashes at different delays after saccade onset (**c**). Blue window: timing of saccades; orange markers: timing of probe flashes.

d. Isolated flash-induced responses (firing rate) of the same RGCs obtained by subtracting responses to saccades-alone (**b**) from responses to saccades followed by probe flashes (**c**). Lines connecting the response peaks highlight the time courses of retinal saccadic suppression relative to baseline flash-induced responses. Numbers above each response peak represent the modulation index which quantifies how much the probe flash response is modulated by the preceding saccade (Methods, negative modulation indices correspond to suppressed flash-induced responses).

e. Population modulation index (mean ± s.e.m.) of ON (light gray) and OFF (dark gray) RGCs, for different background textures with different spatial scales (left to right: fine to coarse). The number of ON and OFF RGCs in the population varied between 68 and 574 for different flash times and textures (see Fig. S3 for exact numbers and relevant statistics). Hash symbols: significant modulation difference between ON and OFF RGCs ($p < 10^{-4}$, two-tailed Wilcoxon rank-sum test).

684 **Figure 2**

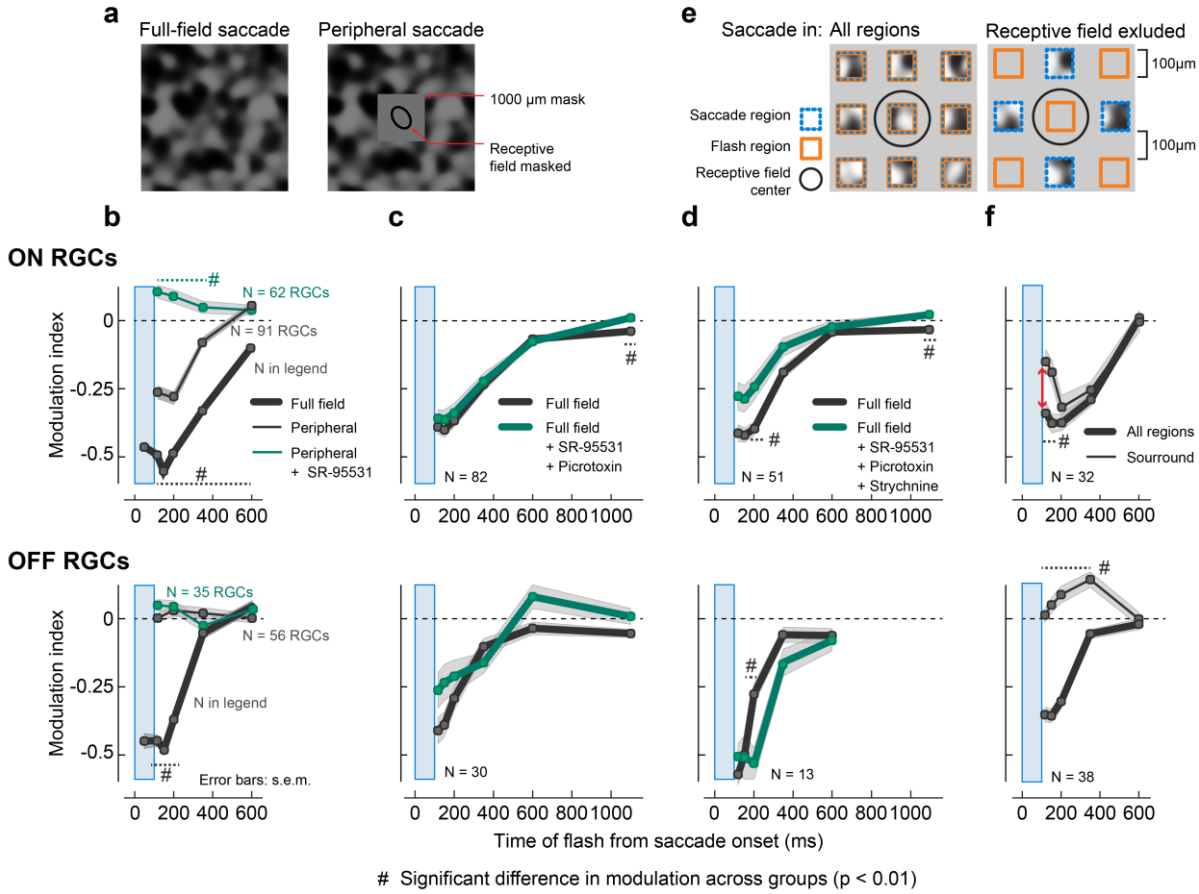

685

686 **Figure 2 Spatial origins of retinal saccadic suppression.**

687 **a.** Spatial layout of the visual stimulation paradigm used in experiments to probe the
688 global component of suppression. Saccades were presented either full-field (left; same
689 as in Fig. 1) or in the periphery (right), where a 1000 x1000 μm^2 mask (intensity: mean
690 luminance of texture) covered at least 2-σ of the 2D Gaussian fit to the RGC receptive
691 fields (Fig. S5b).

692 **b.** Population modulation index (mean ± s.e.m.) of ON (top) and OFF (bottom) RGCs
693 for full-field saccades condition (thick gray lines, same as Fig. 1e rightmost panel;
694 N = 68 to 574 RGCs (see Fig. S3 for exact numbers)); periphery saccades condition
695 (thin gray lines; N = 91 ON RGCs, N = 56 OFF RGCs); and periphery saccades
696 condition in the presence of $GABA_A$ receptor blocker (5µM SR-95531; green lines;
697 N = 62 ON RGCs, N = 35 OFF RGCs). Blue window shows the timing of the saccade.
698 In these experiments, we used a coarse background texture (300 µm spatial scale).
699 Timing of probe flashes: 50 and 150 (only for full-field saccade), 117, 200, 350, 600
700 and 2100 ms (baseline) after saccade onset.

701 **c,d.** Population modulation index (mean ± s.e.m.) of ON (top) and OFF (bottom) RGCs
702 for full-field saccades without any pharmacological agents (gray lines; N = 82 ON
703 RGCs, N = 30 OFF RGCs) and with $GABA_{A,C}$ receptor blockers 5 µM SR-95531 +
704 100 µM Picrotoxin (**c**; green lines), and for a subset of RGCs where we additionally

705 blocked glycine receptors using 1 μM Strychnine (**d**; green lines; N = 51 ON RGCs,
706 N = 13 OFF RGCs). In these experiments, we used a coarse background texture (150
707 μm spatial scale). Probe flashes were presented at 117 ms, 150, 200, 350, 600, 1100
708 and 2100 (baseline) after saccade onset.
709 **e**. Spatial layout of the visual stimulation paradigm used in experiments to probe local
710 components of suppression. Saccades and flashes were presented in 100 x 100 μm^2
711 square regions, separated by 100 μm gaps with mean overall luminance. **Left:**
712 Saccades and flashes were presented in all regions. **Right:** Saccades and flashes
713 were presented in alternate regions; only cells with receptive fields (RFs) in the
714 non-saccade regions (orange) were analyzed (black ellipse: 1-σ of the 2D Gaussian
715 fit to an example RGC receptive field). Consequently, saccades were excluded from
716 at most ~300 x 300 μm^2 of a cell's RF center. In these experiments, we used a coarse
717 background texture (150 μm spatial scale).
718 **f.** Population modulation index (mean ± s.e.m.) of ON (top; N = 32) and OFF (bottom;
719 N = 38) RGCs for saccades and flashes in all regions (thick lines) or saccades
720 excluded from RGC RF center (thin lines). Red arrow indicates significant loss in
721 suppression in ON RGCs for early flashes at 117 and 150 ms upon excluding
722 saccades from RF center ($p = 0.0016$ and $p = 0.002$ respectively; two-tailed Wilcoxon
723 rank-sum test).
724 In all panels, hash symbols indicate statistically significant difference between groups
725 ($p < 0.01$, two-tailed Wilcoxon rank-sum test).
726

727 **Figure 3**

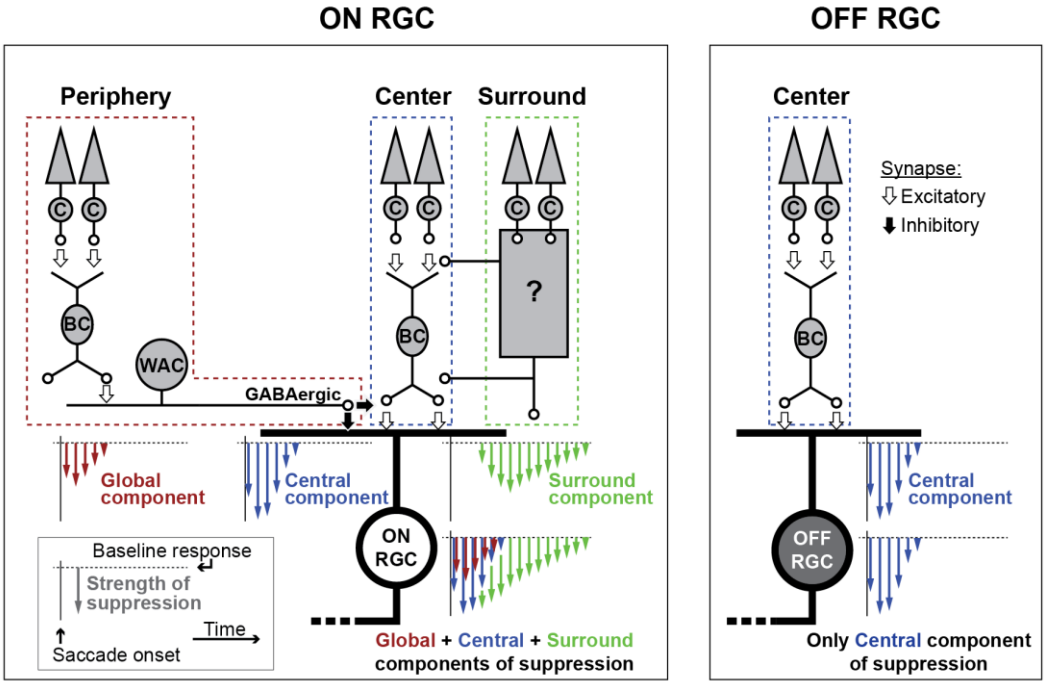

728

729 **Figure 3 Schematic summarizing the spatial origins of retinal saccadic**
730 **suppression.**
731 Saccadic suppression in OFF RGCs (right) is mediated primarily by the central
732 component of suppression (blue) that originates from the cells' receptive field center.
733 ON RGCs (left) get suppressed from two additional components: First, the fast but
734 short-lived global component (red), mediated by GABAergic inhibition, that originates
735 from as far as the cells' periphery. This global component has a similar temporal profile
736 as the central component. It is however weaker than the central component and acts
737 in parallel to it, indicated by the red arrows parallel to blue arrows in the total
738 suppression schematic. Second, the delayed but long-lasting surround component
739 (green), which might originate from the cell's immediate surround. The central
740 component and surround component do not depend on classical GABAergic or
741 glycinergic inhibitory pathways. The differences in the suppression recovery time in
742 ON and OFF RGCs was mainly due to this surround component acting on ON RGCs.
743 Inset shows the legend for arrow schematics. Length of the arrows represent
744 suppression strength; spread of the arrows show the temporal profile of suppression.
745

746 **Figure 4**

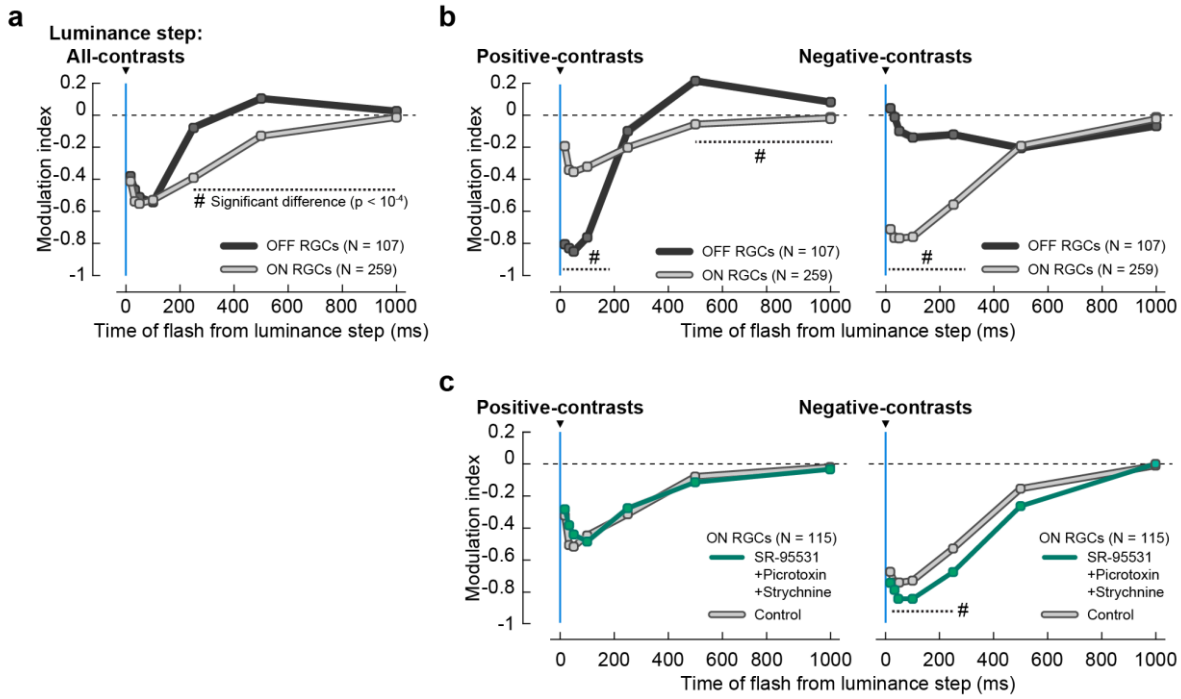

747

748 **Figure 4 Suppression following luminance steps.**

749 **a.** Population modulation index (mean ± s.e.m.) of ON (light gray, N = 259) and OFF
750 (dark gray, N = 107) RGCs for probe flashes following luminance steps (blue line).
751 Modulation index for each RGC was based on its average response to 56 or 156
752 luminance step sequences (Fig. S1b) spanning a contrast range of -0.5 to +0.5
753 Michelson contrast (Methods). Probe flashes were presented at 17 ms, 33, 50, 100,
754 250, 500, 1000 and 2000 (baseline) after luminance steps. Probe flash responses
755 were suppressed in both ON and OFF RGCs, with similar time course and recovery
756 as in the saccade paradigm with textures (Fig. 1e). Error bars are not visible due to
757 small s.e.m.

758 **b.** Same as in **a**, except that the modulation index for each RGC was separately based
759 on average responses to probe flashes after positive-contrast luminance steps (left
760 panel; +0.03 to +0.5 Michelson contrast), and after negative-contrast luminance steps
761 (right panel; -0.03 to -0.5 Michelson contrast). Underlying population data is shown in
762 Fig. S8.

763 **c.** Same as in **b**, for a subset of ON RGCs (N = 115) in control conditions (light gray
764 lines) and with $GABA_{A,C}$ and glycine receptors blocked (green lines; cocktail of 5μM
765 SR-95531, 100 μM Picrotoxin and 1μM Strychnine). Hash symbol: significant
766 difference between modulation of ON and OFF RGCs in **a** or between ON RGCs
767 without and with pharmacological blockers in **c** ($p < 10^{-4}$, two-tailed Wilcoxon rank-sum
768 test).

Figure 5

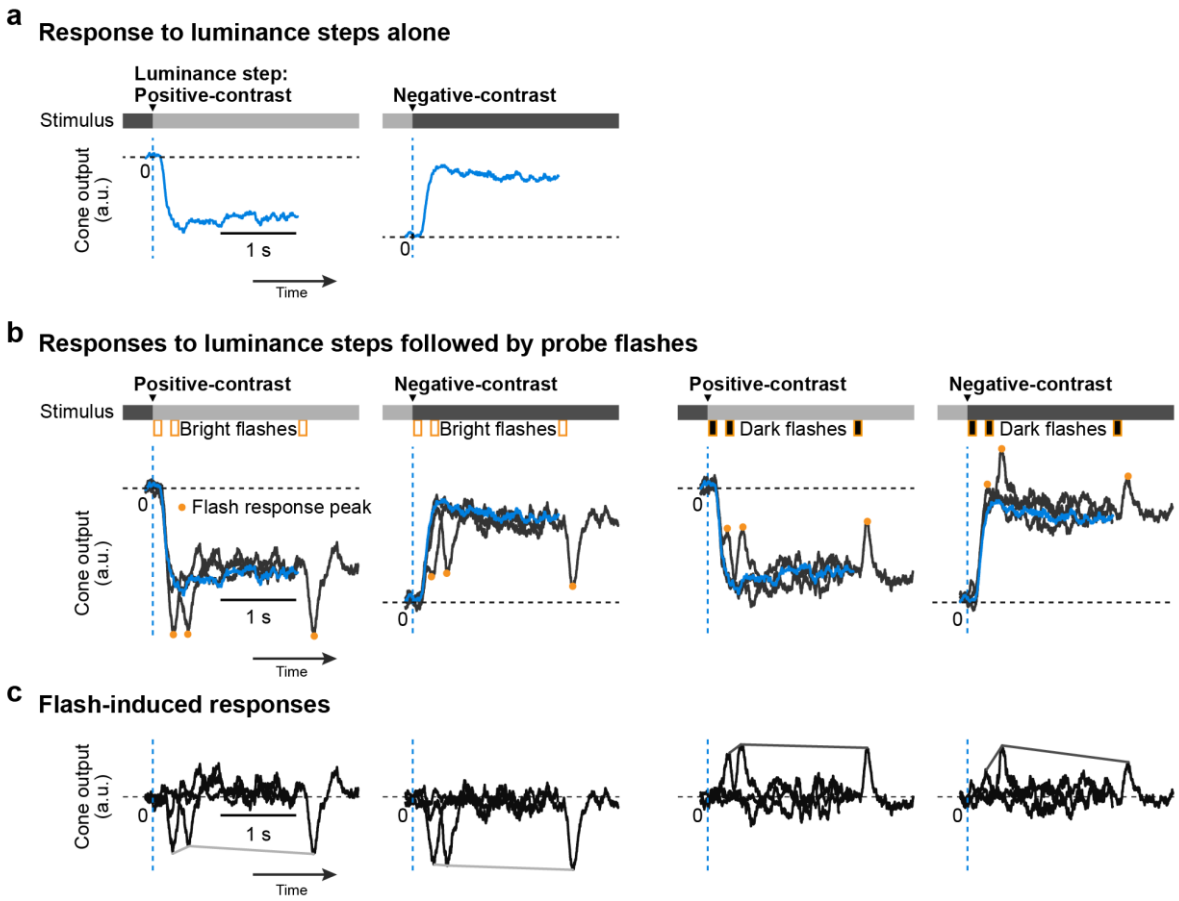

Figure 5 Cone output in response to probe flashes following luminance steps. **a,b.** Cone responses (baseline normalized iGluSnFR indicator fluorescence signal) to positive- and negative-contrast (+0.4 and -0.4 on Michelson scale) luminance steps alone **(a)** and to luminance steps followed by probe flashes at 17, 250 and 2000 ms (orange bars below the intensity bar shows timing of probe flashes) **(b)**. Probe flashes were either bright or dark (+0.33 or -0.33 Michelson contrast respectively; 100 ms long). In **b**, responses to step-alone (blue) and individual step → flash pairs (dark gray) are overlaid. Dashed blue lines: timing of luminance step; orange circles: peak cone response to flashes; horizontal dashed line: cone level prior to the luminance step. **c.** Flash-induced responses, isolated by subtracting luminance step alone responses (blue) from individual composite luminance step-probe flash responses (dark gray) in **b**. Lines connecting the response peaks highlight the time courses of suppression relative to baseline flash-induced (2000 ms) responses.

Figure 6

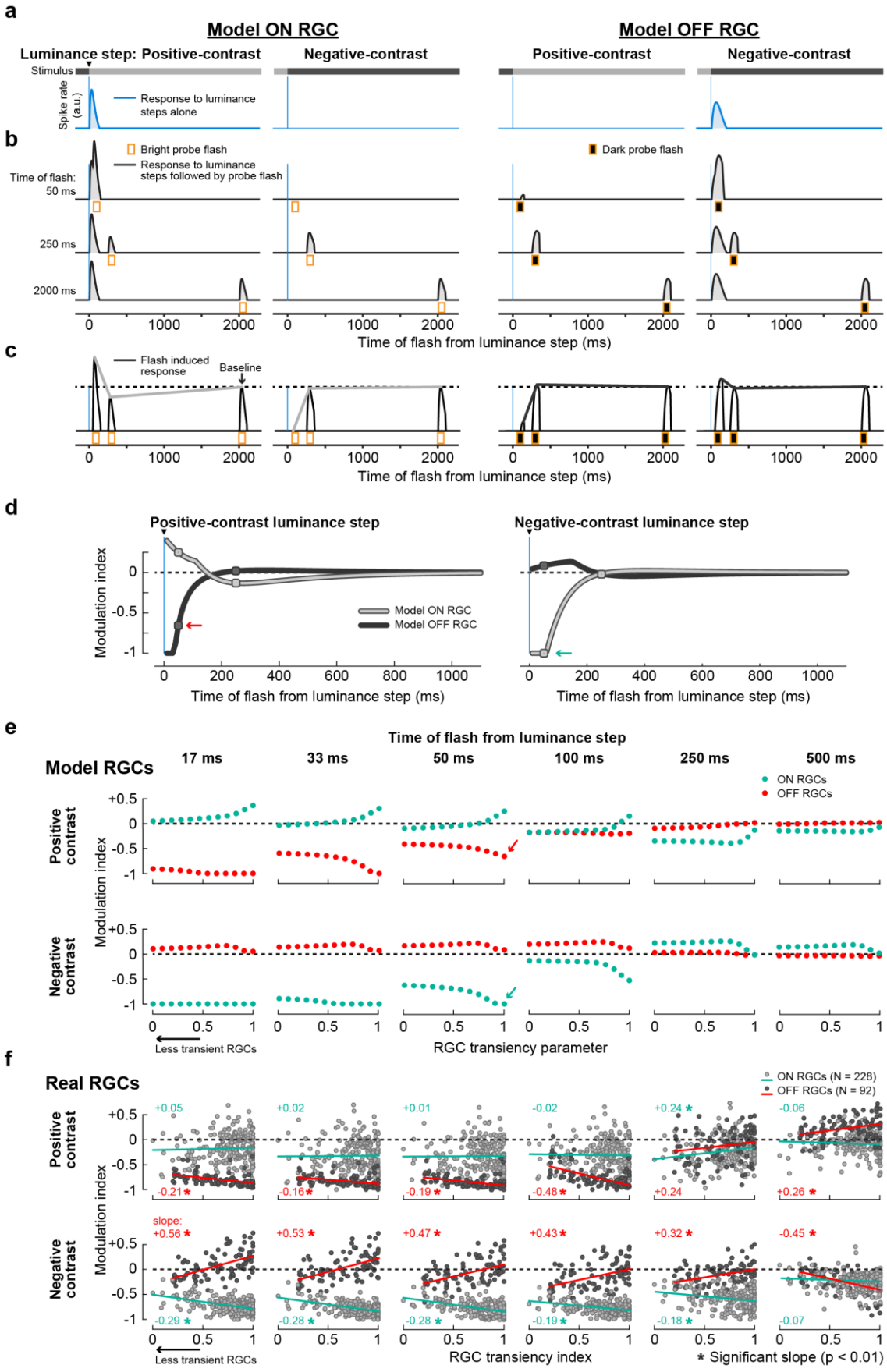
a
Model ON RGC
Model OFF RGC
Luminance step: Positive-contrast
Negative-contrast
Positive-contrast
Negative-contrast
Stimulus
Spike rate (a.u.)
Response to luminance steps alone
b
Bright probe flash
Response to luminance steps followed by probe flash
Dark probe flash
Time of flash: 50 ms
250 ms
2000 ms
Time of flash from luminance step (ms)
c
Flash induced response
Baseline
Time of flash from luminance step (ms)
d
Positive-contrast luminance step
Negative-contrast luminance step
Modulation index
Model ON RGC
Model OFF RGC
Time of flash from luminance step (ms)
e
Time of flash from luminance step
Model RGCs
17 ms
33 ms
50 ms
100 ms
250 ms
500 ms
ON RGCs
OFF RGCs
Positive contrast
Negative contrast
Modulation index
Less transient RGCs
RGC transiency parameter
f
Real RGCs
ON RGCs (N = 228)
OFF RGCs (N = 92)
Positive contrast
Negative contrast
Modulation index
slope:
Less transient RGCs
RGC transiency index
* Significant slope (p < 0.01)

Figure 6 Model RGC responses to probe flashes following luminance steps.
a,b. Spiking response of model ON (columns 1-2) and OFF (columns 3-4) RGCs to luminance steps alone (**a**, blue) and to luminance steps followed by probe flashes (**b**, black) at 50, 250 and 2000 ms (different rows; analogous to real RGCs in Fig. 1b, c). Luminance steps are depicted by intensity bars in **a**. First column in each cell type: responses following a positive-contrast luminance step; second column: responses following a negative-contrast luminance step. Vertical blue lines: timing of luminance step; orange bars: timing of probe flashes. Note the ON RGC and OFF RGC did not spike in response to negative-contrast (column 2) and positive-contrast (column 3) luminance steps respectively.
c. Flash-induced responses, after subtracting **a** from **b**, overlaid to show the modulation of probe flash responses at different times (analogous to real RGCs in Fig. 1d). Lines connecting the response peaks highlight the time courses of suppression relative to baseline flash-induced responses (2000 ms).
d. Modulation indices for probe flashes in ON (light gray) and OFF model RGCs (dark gray), following positive-contrast (left panel) and negative-contrast (right panel) luminance steps. Modulation indices were calculated based on model responses to probe flashes presented at 10 ms intervals after luminance steps, and baseline as response to a flash at 2000 ms. Circle markers indicate modulation indices based on probe flashes at 50 and 250 ms shown in **b, c**. Cyan and red arrows highlight the suppression of opposite-contrast flashes at 50 ms in ON and OFF RGCs, respectively.
e. Modulation indices of model ON (cyan) and OFF (red) RGCs plotted as a function of RGC transiency. Individual panels correspond to different flash times (chosen from real-RGC recordings, Fig. 4) after positive-contrast (top row) and negative-contrast (bottom row) luminance steps. In **a-d**, transiency parameter was set to 1. Arrows highlight the same data as in **d**.
f. Same as in **e** but for real ON (light gray circles; N = 228; cyan line: linear regression fit) and OFF RGCs (dark gray circles; N = 92; red line: linear regression fit). These RGCs are a subset of the population data shown in Fig. 4b for which we could compute a transiency index (Methods). Consistent with model predictions, suppression after negative-contrast steps was weaker in less transient ON RGCs (bottom row, blue regression line has negative slope) and, after positive-contrast steps, suppression was weaker in less transient OFF RGCs (top row, red regression line has negative slope). Numbers in each panel indicate the slope of the fits and asterisk symbol indicates statistically significant slope (slope $\neq 0$, $p < 0.01$, two-tailed t-test).
Fig. S12 shows model RGC responses based on real cone data of Fig. 5 instead of model cone responses.

823 **Figure 7**

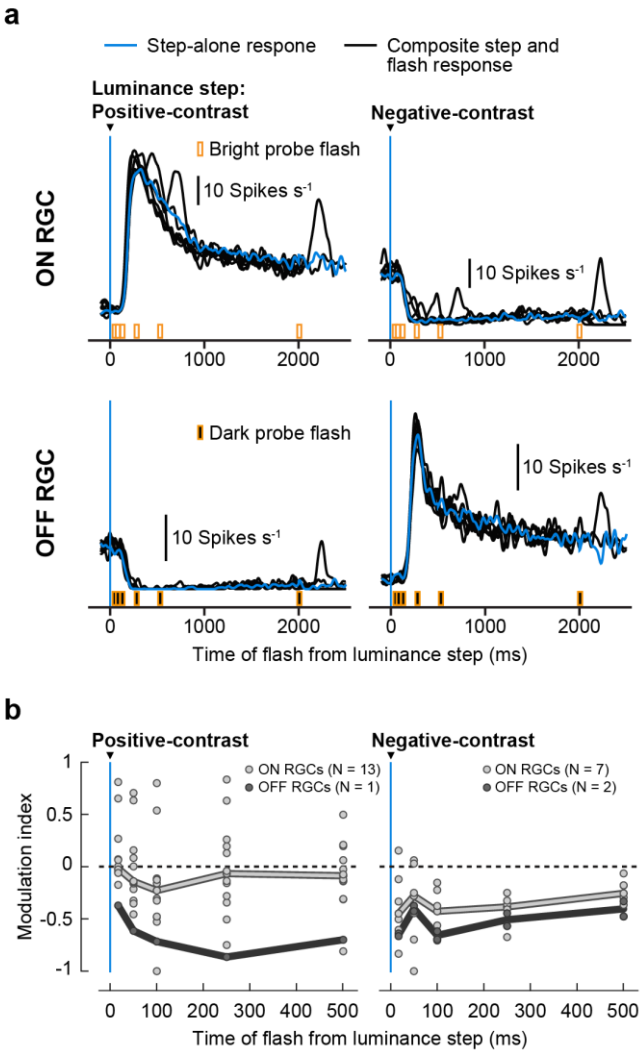

824

825 **Figure 7 Retinal saccadic suppression in Macaque RGCs.**
826 **a.** Average activity of an example macaque ON RGC (top) and OFF RGC (bottom) to
827 positive-contrast (left column) and negative-contrast (right column) luminance steps
828 alone (blue traces) and luminance steps followed by probe flashes (black traces). ON
829 RGCs were analyzed for bright probe flashes and OFF RGCs for dark probe flashes.
830 Responses were averaged across the different positive-contrast (0.05 to 0.5
831 Michelson contrast, N = 10 sequences) and negative-contrast luminance steps (-0.05
832 to -0.5 Michelson contrast, N = 10 sequences).
833 **b.** Median modulation index (thick lines) of macaque ON (light gray) and OFF (dark
834 gray) RGCs for probe flashes presented after positive-contrast (left panel; N = 13 ON
835 RGCs, N = 1 OFF RGC) and negative-contrast luminance steps (right panel; N = 7 ON
836 RGCs, N = 2 OFF RGC). Circles represent modulation indices of individual RGCs.
837 This experiment was performed under scotopic light conditions.

838 **Figure 8**

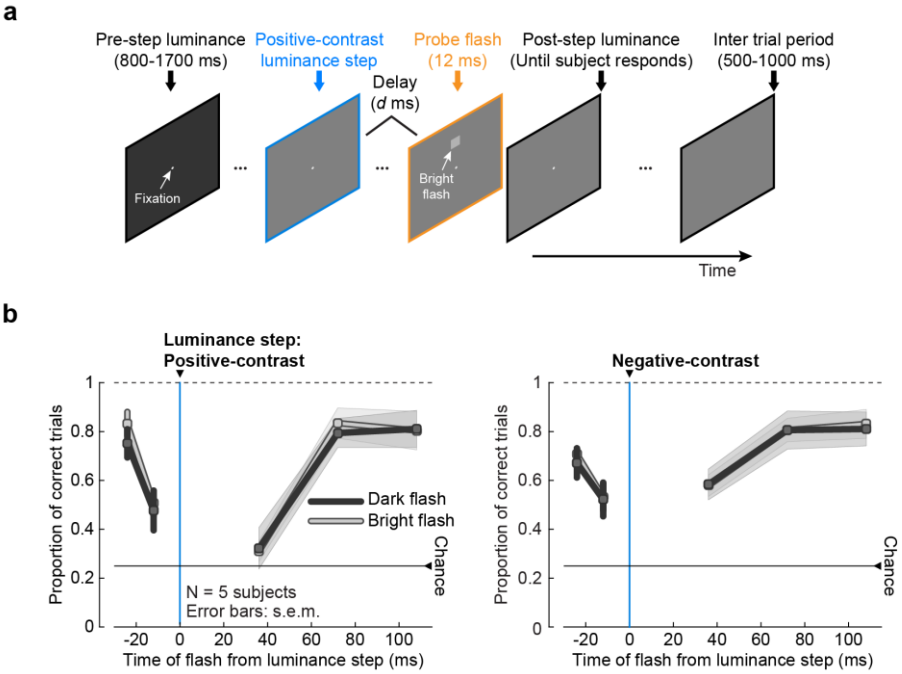

839

840 **Figure 8 Perceptual suppression following luminance steps.**
841 **a.** Example visual task trial. Subjects fixated a small spot on a uniform background
842 with a set luminance (pre-step luminance) for a random duration (800-1700 ms).
843 Background luminance then increased (like shown here) or decreased (positive or
844 negative-contrast luminance step, respectively). At one of 5 times relative to the
845 luminance step (-24, -12, 36, 72, or 108 ms), a luminance pedestal (probe flash,
846 147.8 x 147.8 min arc) was applied for ~12 ms at one of four locations relative to the
847 fixation spot: 7 deg above (shown here), below, to the right, or to the left. The probe
848 flash was brighter (shown here) or darker than the current screen luminance. The
849 background remained at the post-step luminance until the subject responded with the
850 perceived location of the flash, plus an additional 500-1000 ms but without the fixation
851 spot, allowing the subject to relax. The current luminance was the pre-step luminance
852 of the consecutive trial.
853 **b.** Performance of human subjects (mean ± s.e.m., N = 5 subjects), to correctly
854 localize a dark (dark gray) or a bright (light gray) probe flash presented at different
855 times relative to positive-contrast (left panel) and negative-contrast (right panel)
856 luminance steps (blue line). Each subject's responses were averaged across the
857 different positive-contrast (0.3 to 0.56 Michelson contrast) and negative-contrast (-0.3
858 to -0.56 Michelson contrast) luminance steps. Perceptual performance was reduced
859 around the time of luminance steps, reflecting suppression, irrespective of the
860 combination of luminance step polarity and flash polarity. There were no statistically
861 significant differences in suppression of dark and bright probe flashes (two-tailed
862 Wilcoxon rank-sum test). Note that in the right panel, the suppression profile for bright
863 probe flashes almost completely overlaps the suppression profile of dark probe
864 flashes.

865 # METHODS

866 ## Experimental model and subject details

867 ### Animals

868 We performed electrophysiological experiments on ex vivo mouse, pig and macaque
869 retinae; and imaging experiments on ex vivo mouse retinae.

870 Mouse and pig ex vivo retinae experiments were performed in Tübingen, in
871 accordance with German and European regulations, and animal experiments were
872 approved by the Regierungspräsidium Tübingen. Macaque ex vivo retina experiment
873 was performed at Stanford University. Eyes were removed from a terminally
874 anesthetized macaque rhesus monkey used by other laboratories in the course of their
875 experiments, in accordance with the Institutional Animal Care and Use Committee
876 guidelines of Stanford University.

877 For mouse retina electrophysiology, we used 47 retinae from 15 male and 30 female
878 *PV-Cre x Thy-S-Y* mice (*B6;129P2-Pvalb*$^{tm1(cre)Arbr}$*/J × C57BL/6-tg (ThystopYFPJS))*,
879 3-12 months old, which are functionally wild type (Farrow et al., 2013; Münch et al.,
880 2009; Tikidji-Hamburyan et al., 2015). Additionally, we recorded the cone output from
881 4 retinae obtained from two C57BL/6 male mice, 9 to 10 weeks old. We housed mice
882 on a 12/12 h light/dark cycle, in ambient temperatures between 20-22 °C and humidity
883 levels of 40%.

884 We also replicated experiments on 9 pig retinae obtained from domestic female pigs
885 after they had been sacrificed during independent studies at the Department of
886 Experimental Surgery at the Medical Faculty of the University of Tübingen. Pigs were
887 anesthetized using atropine, azaperone, benzodiazepine (midazolam), and ketamine,
888 and then sacrificed with embutramide (T61). Before embutramide administration,
889 heparin was injected.

890 One experiment was conducted with a retina extracted from a macaque rhesus
891 monkey.

892 **Humans**

893 Human psychophysics experiments were performed in Tübingen. Human subjects
894 provided written, informed consent, and they were paid 10 Euros per session of 60
895 minutes each, for three sessions. Human experiments were approved by ethics
896 committees at the Medical Faculty of Tübingen University, and they were in
897 accordance with the Declaration of Helsinki.

898 In total, we collected data from 5 subjects (24-29 years old; one female).

899 Experimental setup

900 **Retina electrophysiology (mouse and pig): procedure and laboratory setup**

901 Mice were dark adapted for 4-16 h before experiments. We then sacrificed them under
902 dim red light, removed the eyes, and placed eyecups in Ringer solution (in mM: 110
903 NaCl, 2.5 KCl, 1 $CaCl_2$, 1.6 $MgCl_2$, 10 D-glucose, and 22 $NaHCO_3$) bubbled with 5%
904 CO_2 and 95% O_2. We removed the retina from the pigment epithelium and sclera while
905 in Ringer solution.

906 Pigs were dark-adapted for 15-20 min before sacrifice. Immediately after
907 veterinary-confirmed sacrifice, the eyes were enucleated under dim red light, and the
908 cornea, lens, and vitreous were removed. Eyecups were kept in CO_2-independent
909 culture medium (Gibco) and protected from light. We transported eyecups to our
910 laboratory and cut pieces from mid-peripheral or peripheral retinae. Only those retinae
911 which showed ganglion cell responses to light stimuli were used in our experiments.

912 We recorded mouse and pig retinal ganglion cell (RGC) activity using either low- or
913 high-density multi-electrode arrays (MEAs). The low-density setup consisted of a
914 perforated 60-electrode MEA (60pMEA200/30ir-Ti-gt, Multichannel Systems (MCS),
915 Reutlingen, Germany) having a square grid arrangement and 200 μm inter-electrode
916 distance. We whole mounted an isolated retina on a nitrocellulose filter (Millipore) with
917 a central 2 x 2 mm hole. The mounted retina was placed with the RGC side down into
918 the recording chamber, and good electrode contact was achieved by negative
919 pressure through the MEA perforation. We superfused the tissue with Ringer solution
920 at 30-34 °C during recordings, and we recorded extracellular activity at 25 kHz using

921 a USB-MEA-system (USB-MEA 1060, Multichannel Systems) or a memory-card
922 based system (MEA1060, Multichannel Systems). Data was acquired using MC Rack
923 version 4.6.2 (Multichannel Systems). A detailed step-by-step approach is provided in
924 (Reinhard et al., 2014).

925 The high-density MEA setup consisted of either a HiDens CMOS MEA (Frey et al.,
926 2009) (developed by the lab of Andreas Hierlemann, Basel, Switzerland) or a MaxOne
927 system (Müller et al., 2015) (Maxwell Biosystems, Basel, Switzerland). The HiDens
928 CMOS MEA featured 11,011 metal electrodes with inter-electrode (center-to-center)
929 spacing of 18 μm placed in a honeycomb pattern over an area of 2 x 1.75 mm. Any
930 combination of 126 electrodes could be selected for simultaneous recording. The
931 MaxOne MEA featured 26,400 metal electrodes with center-to-center spacing of 17.5
932 μm in a grid-like arrangement over an area of 3.85 x 2.1 mm. In this system, up to
933 1024 electrodes could be selected for simultaneous recordings. For each experiment,
934 a piece of isolated retina covering almost the entire electrode array was cut and placed
935 RGC-side down in the recording chamber. We achieved good electrode contact by
936 applying pressure on the photoreceptor side of the retina by carefully lowering a
937 transparent permeable membrane (Corning Transwell polyester membrane, 10 μm
938 thick, 0.4 μm pore diameter) with the aid of a micromanipulator. The membrane was
939 drilled with 200 μm holes, with center-center distance of 400 μm, to improve access
940 of the Ringer solution to the retina. We recorded extracellular activity at 20 kHz using
941 FPGA signal processing hardware. In the case of the HiDens CMOS MEA, data were
942 acquired using custom data acquisition software, called MEA 1k Scope (developed by
943 the lab of Andreas Hierlemann, Basel, Switzerland). In the case of the MaxOne MEA,
944 data were acquired using MaxLab software provided by Maxwell Biosystems, Basel,
945 Switzerland.

946 In total, we performed 59 recordings, 47 from mouse and 12 from pig retinae. 24 of
947 the 59 recordings were done using low-density MEAs. Once a basic experimental
948 protocol was established, we shifted to HiDens CMOS MEA providing much higher
949 throughput. 12 experiments were done using this setup. We upgraded to the MaxOne
950 MEA for even higher throughput and did 23 recordings using this setup. A subset of
951 the data collected from 32 of the 59 recordings (20 from mouse and 12 from pig

952 retinae), was also used in our previous study (Idrees et al., 2020). Here, we show
953 further in-depth analysis of that data.

954 We presented light stimuli to the retinal piece that was placed on the MEA using a DLP
955 projector running at 60 Hz (Acer K11 for low-density MEA experiments and Lightcrafter
956 4500 from EKB Technologies Ltd. with internal red, green and blue light-emitting
957 diodes, for high-density MEA experiments). 60 Hz is above the flicker fusion frequency
958 of both mouse and pig retinae; therefore, the framerate of these projectors was
959 adequate for our purposes. The Acer K11 projector had a resolution of 800 x 600
960 pixels covering 3 x 2.25 mm on the retinal surface. Lightcrafter 4500 had a resolution
961 of 1280 x 800 pixels, extending 3.072 x 1.92 mm on the retinal surface. We focused
962 images onto the photoreceptors using a condenser (low-density MEA recordings,
963 illumination from below) or a 5x objective (high-density MEAs, illumination from
964 above). In each case, the light path contained a shutter and two motorized filter wheels
965 with a set of neutral density (ND) filters (Thorlabs NE10B-A to NE50B-A), having
966 optical densities from 1 (ND1) to 5 (ND5). The filters allowed us to adjust the absolute
967 light level of the stimulation.

968 We measured the spectral intensity profile (in μW cm^{-2} nm^{-1}) of our light stimuli with a
969 calibrated USB2000+ spectrophotometer (Ocean Optics) and converted the physical
970 intensity into a biological equivalent of photoisomerizations per rod photoreceptor per
971 second (R*rod^{-1}s^{-1}), as described before (Tikidji-Hamburyan et al., 2015). Light
972 intensities of the projector output covered a range of 3 log units (i.e. 1000-fold
973 difference between black and white pixels, over an 8-bit range). We linearized the
974 projector output, and we used only grayscale images of limited contrast, spanning at
975 most the range from 0 to 120 in the 8-bit range of the projector (see stimulus
976 description below for details). Absolute light intensities were set to the mesopic level,
977 where a stimulus intensity of '30' in our 8-bit DLP projector scale (0-255) corresponded
978 to 225 to 1000 R*rod^{-1}s^{-1}, depending on the experimental rig used for the experiment
979 (i.e. different DLP projectors and MEAs). We pooled all data from the different rigs as
980 separate individual analyses from the individual setups revealed no effects of
981 recording conditions in the different setups. For experiments of Fig. S4, we also
982 recorded at scotopic light levels where a stimulus intensity of '30', corresponded to 23
983 R*rod^{-1}s^{-1} at scotopic level.

984 **Retina electrophysiology (macaque): procedure and laboratory setup**

985 In one experiment, we recorded the activity of macaque retinal ganglion cells. For this
986 experiment we used a high-density MEA, as described previously (Chichilnisky and
987 Baylor, 1999; Field et al., 2007). Following enucleation, the anterior portion of the eye
988 and vitreous were removed. The eye was stored in a dark container in oxygenated
989 Ames' solution (Sigma, St. Louis, MO) at 33°C, pH 7.4. Under infrared illumination, a
990 small piece of retina approximately 1x1 mm, from a retinal region with eccentricity
991 around 12 mm (4.0-17mm temporal equivalent eccentricity; (Chichilnisky and Kalmar,
992 2002)), was dissected and placed ganglion cell side down on a MEA for recording.
993 The retina pigment epithelium remained attached during the recording; the retina was
994 perfused with oxygenated Ames' solution. A custom planar large-scale MEA (Field et
995 al., 2007; Litke et al., 2004) with a hexagonal outline of 519 electrodes at 30 μm pitch
996 was used. Recorded voltages were band-pass filtered, amplified, and digitized at 20
997 kHz using custom electronics (Litke et al., 2004). Spike sorting process was described
998 previously (Field et al., 2007).

999 Visual stimulation was performed with the optically reduced image of a
1000 gamma-corrected OLED microdisplay (eMagin) refreshing at 60.35 Hz focused on the
1001 photoreceptor outer segments. The visual stimulus was delivered through the
1002 mostly-transparent electrode array. The power of each display primary was measured
1003 at the preparation with a calibrated photodiode (UDT Instruments). At the mean
1004 background illumination level, the photoisomerization rates for the rods and the L, M,
1005 and S cones were approximately 29, 9, 9, and 2 $P^{*}receptor^{-1}s^{-1}$, respectively (see Li
1006 et al., 2014), placing the retina in scotopic regime.

1007 **Retina electrophysiology: pharmacology**

1008 In several MEA experiments, we used pharmacological agents to block specific
1009 receptors in the mouse retina. To block $GABA_A$ receptors selectively, we used 5 μM
1010 SR-95531 (gabazine, an antagonist of $GABA_A$ receptors; Sigma). To block both
1011 $GABA_A$ and $GABA_C$ receptors, we used 100 μM picrotoxin (an antagonist of $GABA_A$
1012 and $GABA_C$ receptors; Sigma). To block glycine receptors, we used 1 μM Strychnine
1013 (antagonist of Glycine receptors).

1014 We first prepared a 1000x stock solution of these pharmacological blockers as follows:
1015 SR-95531 was dissolved in water at a concentration of 5 mM; picrotoxin was dissolved
1016 in DMSO at a concentration of 100 mM; Strychnine was dissolved in Chloroform at a
1017 concentration of 1mM. During the experiments, we pipetted the stock solution to the
1018 Ringer solution in a 1:1000 ratio. Wash-in was performed for 20 min.

1019 **Cone photoreceptors imaging: procedure and laboratory setup**

1020 To record the output of cone photoreceptors in the mouse retina, we measured the
1021 glutamate release using an intensity based glutamate-sensitive fluorescent reporter,
1022 iGluSnFR (Marvin et al., 2013) expressed in horizontal cell processes post-synaptic to
1023 cone terminals, using a viral approach. We recorded the cone output from 4 retinae
1024 obtained from two C57BL/6 male mice, 9 to 10 weeks old. Below, we reproduce the
1025 methods, previously described in Szatko et al (Szatko et al., 2020).

1026 We dark-adapted the mice for ≥1 h before the experiments. They were then
1027 anaesthetized using isoflurane (Baxter) and sacrificed by cervical dislocation. The
1028 eyes were enucleated and hemisected in carboxygenated (95% O_2 and 5% CO_2)
1029 artificial cerebrospinal fluid (ACSF) solution containing (in mM): 125 NaCl, 2.5 KCl, 2
1030 $CaCl_2$, 1 $MgCl_2$, 1.25 NaH_2PO_4, 26 $NaHCO_3$, 20 glucose, and 0.5 L-glutamine (pH
1031 7.4). We then moved the tissue to the recording chamber where it was continuously
1032 perfused with carboxygenated ACSF at ~36 °C. In these experiments, ACSF
1033 contained ~0.1 μM Sulforhodamine-101 (SR101, Invitrogen) to reveal blood vessels
1034 and any damaged cells in the red fluorescence channel (Euler et al., 2019). All
1035 procedures were carried out under very dim red (>650 nm) light.

1036 iGluSnFR was expressed in the retina by viral transduction of
1037 AAV2.7m8.hSyn.iGluSnFR, generated in the Dalkara lab (Institut de la Vision) as
1038 described in (Dalkara et al., 2013; Khabou et al., 2016). The iGluSnFR plasmid
1039 construct was provided by J. Marvin and L. Looger (Janelia Research Campus, USA).
1040 A volume of 1 μL of the viral construct was injected into the vitreous humour of the
1041 mice, anaesthetized with 10% Ketamine (Bela-Pharm GmbH & Co. KG) and 2%
1042 xylazine (Rompun, Bayer Vital GmbH) in 0.9% NaCl (Fresenius). For the injections,
1043 we used a micromanipulator (World Precision Instruments) and a Hamilton injection

1044 system (syringe: 7634-01, needles: 207434, point style 3, length 51 mm, Hamilton
1045 Messtechnik GmbH). Imaging experiments were performed 3-4 weeks after injection.
1046 In the outer retina, iGluSnFR was predominantly expressed in horizontal cells. As the
1047 expression tended to be weaker in the central retina, most scan fields were acquired
1048 in the medial to peripheral ventral or dorsal retina.

1049 To record the iGluSnFR signal, we used a MOM-type two-photon microscope setup
1050 (designed by W. Denk, MPI, Heidelberg; purchased from Sutter Instruments / Science
1051 Products). The design and procedures have been previously described in (Euler et al.,
1052 2009, 2019). In brief, the system was equipped with a mode-locked Ti:Sapphire laser
1053 (MaiTai-HP DeepSee, Newport Spectra-Physics), two fluorescence detection
1054 channels for iGluSnFR (HQ 510/84, AHF/Chroma) and SR101 (HQ 630/60, AHF), and
1055 a water immersion objective (W Plan-Apochromat 20x /1.0 DIC M27, Zeiss). The laser
1056 was tuned to 927 nm for imaging iGluSnFR. For image acquisition, we used custom
1057 made software (ScanM by M. Müller and T. Euler) running under IGOR Pro 6.3 for
1058 Windows (Wavemetrics), taking time-lapsed 128 x 128 pixel image scans at 3.9 Hz in
1059 the outer plexiform layer (OPL).

1060 For light stimulation in cone imaging experiments, we used the Lightcrafter (LCr;
1061 DPM-E4500UVBGMKII), a DLP projector from EKB Technologies Ltd. with internal UV
1062 and green light-emitting diodes (LEDs). The light from the DLP projector was focused
1063 through the objective. To optimize spectral separation of mouse M- and S- opsins,
1064 LEDs were band-pass filtered (390/576 Dualband, F59-003, AHF/Chroma). LEDs of
1065 the DLP projector were synchronized with the microscope's scan retrace. Stimulus
1066 intensity (as isomerization rate, $P^{*}cone^{-1}s^{-1}$) was calibrated to range from ~500 (black
1067 image) to ~20,000 for M- and S-opsins. In addition, a steady illumination component
1068 of ~10^4 $P^{*}cone^{-1}s^{-1}$ was present during the recordings because of two-photon
1069 excitation of photopigments. The overall light intensity falling on to the retina was
1070 therefore in the low photopic regime. The light stimulus was centered to the recording
1071 field before every experiment. For all experiments, the retinal tissue was kept at a
1072 constant mean stimulator intensity level for at least 15 s after the laser scanning started
1073 and before stimuli were presented.

Human psychophysics: laboratory setup

We used a similar laboratory setup as described previously (Idrees et al., 2020). Briefly, subjects sat in a dark room 57 cm in front of a CRT monitor (85 Hz refresh rate; 41 pixels per deg resolution) spanning 34.1 x 25.6 deg (horizontal x vertical). Head fixation was achieved with a custom head, forehead, and chin rest (Hafed, 2013), and we tracked eye movements of the left eye at 1 kHz using a video-based eye tracker (EyeLink 1000, SR Research Ltd, Canada). Gray backgrounds in the luminance step experiment (Fig. 8) were always presented at an average luminance of 49.84 cd m^{-2}, and the monitor was linearized (8-bit resolution) such that equal luminance increments and decrements for luminance steps were possible around this average. In total, we collected data from 5 subjects (24-29 years old; one female). A subset of the data from 4 subjects was used in our previous study (Idrees et al., 2020). Here, we perform novel analyses of the complete dataset, in addition to one new subject.

Visual stimuli: Retina electrophysiology (Figs. 1-4, 7, S3-S10, S13)

In retina electrophysiology experiments, we used two broad visual stimulation paradigms: a saccade (texture displacements) paradigm (Fig. S1a), and a luminance step paradigm (Fig. S1b), described in detail below. In different experiments we used different spatial and/or pharmacological manipulations of these two paradigms.

Saccade (texture displacements) paradigm

<u>Background textures</u>

We created background textures (Fig. S2a) by convolving a random binary (i.e. white or black) pixel image with a two-dimensional Gaussian blurring filter (Schwartz et al., 2012) defined by the kernel

$$G(x,y) = e^{\frac{-(x^2+y^2)}{2\sigma^2}} \qquad \text{(Equation 1)}$$

The parameter σ of the kernel influenced the amount of blurring. This resulted in textures having effectively low-pass spectral content (Fig. S2b) with a cutoff frequency depending on σ. For easier interpretation, we define the spectral content of these textures by a spatial scale. Intuitively, the spatial scale approximates the size of the

1103 smallest dark and bright image blobs of the texture (Fig. S2a). Quantitatively, the
1104 spatial scale is defined as the $2*\sigma$ parameter of the Gaussian blurring filter. We
1105 generated textures with four different spatial scales: 25, 50, 150 and 300 μm, that
1106 resulted in dark and bright image blobs approximating a range of receptive field sizes
1107 between bipolar cells (texture with spatial scale 25 μm, see (Zhang et al., 2012)) and
1108 RGCs (textures with spatial scale 150 and 300 μm). In other words, coarser textures
1109 matched the resolution of RGCs, and finer textures matched the resolution of one
1110 processing stage earlier, the retinal bipolar cells. Calculating power spectra for the
1111 textures (Fig. S2b) confirmed that the spatial scale and hence the cutoff frequencies
1112 were consistent with this design aim. In different experiments, we used textures of all
1113 or a subset of the different spatial scales.

1114 We normalized the pixel intensities in the textures to have uniform variations in
1115 luminance around a given mean. We used pixel intensities (from our 8-bit resolution
1116 scale) ranging from 0 to 60 around a mean of 30, or ranging from 30 to 90 around a
1117 mean of 60 (see sub-section *Saccades and probe flashes* for when each paradigm
1118 was used).

1119 Saccades and probe flashes

1120 To simulate saccades in our ex vivo retina electrophysiology experiments, we
1121 displaced the texture across the retina in 6 display frames (100 ms at 60 Hz refresh
1122 rate). For easier readability, we usually refer to these saccade-like texture
1123 displacements as “saccades”. The textures were displaced in each frame by a
1124 constant distance along a linear trajectory. While each “saccade” lasted 100 ms,
1125 displacement direction was varied randomly for each “saccade” (uniformly distributed
1126 across all possible directions), and “saccade” amplitude could range from 310 μm to
1127 930 μm (corresponding to a velocity range of 3100-9300 μm s^{-1} on the retinal surface).
1128 In visual degrees, this corresponds to a velocity range of 100-300 deg s^{-1} and
1129 displacement range of 10-30 deg in mice, well in the range of observed mouse
1130 saccade amplitudes (Sakatani and Isa, 2007). Similar to primates, mice also have
1131 oculomotor behavior, even under cortical control (Itokazu et al., 2018). For example,
1132 they make, on average, 7.5 saccade-like rapid eye movements per minute when their
1133 head is fixed (Sakatani and Isa, 2007) (humans make several saccades per second).

1134 We used the same retinal displacement range of 310 μm to 930 μm for pig retinae. To
1135 the best of our knowledge, pig oculomotor behavior has not been documented in the
1136 literature. However, with their larger eyeball sizes, our translations of the retinal image
1137 would correspond to slower saccades (e.g. small saccades in humans and monkeys),
1138 which are also associated with saccadic suppression. Moreover, retinal "saccadic
1139 suppression" is not critically dependent on the details of movement kinematics, as it is
1140 triggered by visual transients (Fig. 4, also see Figs. 4, 5 in Idrees et al., 2020).

1141 Each trial consisted of successive sequences (Fig. 1a, S1a) that combined a
1142 "saccade" with a probe flash, as follows: there was first a "pre-saccade" fixation of 2
1143 seconds, where the texture remained static over the retina, then a 100 ms "saccade",
1144 followed by "post-saccade" fixation where the texture again remained static over the
1145 retina but now with a shifted texture. At a certain time from "saccade" onset (delay *d*,
1146 range: 50 ms to 2100 ms), we presented a probe flash (see below). Following the
1147 probe flash, the texture remained static at the post-saccade fixation position for
1148 another 2 seconds before the next saccade of the successive sequence occurred. The
1149 post-probe-flash fixation of one sequence was therefore also the pre-saccade fixation
1150 of the next sequence. This way the texture remained visible during the entire trial,
1151 being translated during saccades of the successive sequences. In a single trial, 39
1152 such sequences occurred. In each successive sequence, the direction and amplitude
1153 of the saccade was pseudo-randomly determined by the range of allowed saccade
1154 amplitudes and directions. The texture always landed at unique locations within a trial.
1155 The end result was that, within a single trial, RGCs experienced a wide spectrum of
1156 saccade amplitudes, directions and contrasts across these 39 saccades. As such, by
1157 analyzing the average effects of the 39 saccades on RGC responses to probe flashes,
1158 we captured a wide range of saccade-induced kinematics and luminance changes
1159 over the RGC receptive fields.

1160 In most cases, the probe flash had a duration of 2 frames (~33 ms). We used 1 frame
1161 (~16 ms) in a subset of earlier experiments (mouse: 709 of 1616 cells; pig: 116 of 228
1162 cells). Results were pooled across these paradigms as the effects were
1163 indistinguishable. The probe flash was a full-screen positive ("bright") or negative
1164 ("dark") stimulus transient.

Bright or dark probe flashes could happen in two different ways across our experiments. The results were indistinguishable between the two ways, so we pooled results across them. Briefly, in one manipulation, the probe flash replaced the texture with a homogeneous bright (pixel intensity of 60 in our 8-bit projectors) or dark (pixel intensity of 0) full-screen (in these experiments, the textures themselves had intensities ranging from 0 to 60 pixel intensity; see *Background textures* above). This way, the flash contrast from the underlying background luminance was variable across space (e.g. a bright flash on a bright portion of a texture had lower contrast from the underlying texture than the same flash over a dark portion of the texture). In the second manipulation, the bright and dark flashes were simply luminance increments or decrements (by pixel values of 30 on our 8-bit projectors) over the existing textures. This way, spatial contrast relationships in the background textures were maintained. In these experiments, the textures themselves had a range of 30-90 pixel intensities and a mean pixel value of 60 (on our 8-bit projectors). Out of the 1616 RGCs that we analyzed for saccadic suppression across all experiments where texture displacements were used as saccades (irrespective of the spatial or pharmacological manipulations), 1129 RGCs experienced such probe flashes, whereas the rest (487 RGCs) experienced the homogenous probe flash. For pig retina recordings, we always used the homogenous framework. However, in the subset of pig experiments where the 2-frame probe flash was employed (112 of 228 RGCs), we used a high-contrast probe flash such that a bright flash would be achieved by first going to 0 in the first frame of the flash then going to 60 (on our 8-bit projectors) in the next frame (and vice versa for a dark flash). Again, all data were pooled across these different paradigms because their outcomes were indistinguishable.

The number of trials required during a physiology experiment depended on the number of conditions that we ran on a specific day. For example, testing 7 different flash delays required 15 trials (7 with bright probe flashes, 7 with dark probe flashes, and 1 without probes). In a given experiment, we always interleaved all the conditions; that is, in any one of the 15 necessary trials, each of the 39 saccades could be followed by a bright or a dark probe at any of the 7 delays, or no probe flash at all (Fig. S1a shows schematic of one such trial). Moreover, we repeated the total number of conditions (e.g. the interleaved 15 trials) 4 times per session, and we averaged responses across

1197 those repetitions. Since one trial typically lasted for 2 minutes, the example of 15 trials
1198 repeated 4 times lasted for approximately 2 hours. This was usually combined with
1199 additional conditions (e.g. other background texture scales). Therefore, the total
1200 number of saccades shown in any given experiment could be computed by #trials x 39
1201 saccades per trial x #textures x #repetitions. A typical experiment lasted 10-12 hours.
1202 If the combination of conditions would have required even longer recordings in a given
1203 experiment, we reduced the number of conditions (e.g. we presented flashes at fewer
1204 delays, or used fewer texture scales).

1205 Full-field saccades

1206 In the full-field saccades experiments, saccades and probe flashes occurred over the
1207 entire retina. This was our main experimental paradigm that we used for characterizing
1208 how saccades modulate RGC responses to probe flashes. This paradigm was also
1209 used as a control in experiments in which we applied different spatial or
1210 pharmacological manipulations of this paradigm to probe for the spatial origins and
1211 mechanisms of saccadic suppression. Further, results from this paradigm served as a
1212 baseline standard across different experimental rigs. This paradigm was used in a total
1213 of 32 retinal recordings (32 retinae from 30 mice). In different recordings, we used a
1214 subset of the texture scales and probe flash delays. This explains the different values
1215 of N seen for different conditions in, for example, Figs. 1e, S3. However, to ensure
1216 comparison, some conditions always overlapped across different recordings. This
1217 paradigm was also used in 12 recordings with retinae from 6 pigs.

1218 Periphery saccades (global component of suppression)

1219 In this manipulation, we restricted saccades to the RGC's receptive fields periphery
1220 (i.e. its far surround). This spatial manipulation was used to investigate the spatial
1221 origins of the global component of suppression (Figs. 2a-b, S5). We performed 13
1222 recordings (13 retinae from 13 mice) with this paradigm, always with the high-density
1223 multielectrode array system (MaxOne by MaxWell), as it provided a large electrode
1224 area (~2 x 4 mm^2) for the retina to be placed on. The recording region was typically
1225 either a high density block of electrodes (inter-electrode spacing: ~17.5 μm) or a block
1226 with one-electrode spacing (inter-electrode spacing: ~35 μm). The recording region
1227 was selected close to the center of the electrode array. We centered a large square
1228 mask (1000 x 1000 μm^2) over the recording region to restrict the texture and saccade

1229 presentation to the periphery of RGC receptive fields (Fig. S5b). The mask had a
1230 homogenous intensity corresponding to the mean luminance of the texture. At different
1231 times relative to texture displacements, full-field probe flashes were presented, similar
1232 to experiments with full-field texture displacements. The intensity of each pixel of the
1233 stimulus (both the mask and the texture regions) was adjusted for the probe flashes,
1234 either decreased or increased by a pixel value of 30 (on our 8-bit projectors) for dark
1235 and bright probe flashes, respectively. In all periphery saccade experiments, we used
1236 probe flash duration of ~33 ms, and a coarse texture background of spatial scale 300
1237 μm.

1238 Checkerboard mask paradigm (local component of suppression)
1239 In this spatial manipulation we presented saccades and flashes in small square
1240 regions spread equidistantly over the entire retina. Each square region measured
1241 100 x 100 μm^2, separated from adjacent squares by an edge-edge gap of 100 μm.
1242 The gap was kept at mean luminance throughout the experiment. Saccades and
1243 flashes could either be presented in all the regions (similar to full-field saccades,
1244 except for the gap), or in alternate regions (Fig. 2e, S7a), arranged like in a
1245 checkerboard. This paradigm was used to investigate the origins of the local
1246 component of suppression (Figs. 2f, S7a-c). We performed 4 recordings (4 retinae
1247 from 3 mice) with this paradigm, always with the low density MCS MEA rig. In all
1248 experiments with this spatial manipulation, we used probe flash duration of ~17 ms,
1249 and a coarse texture background of spatial scale of 150 μm.

1250 ***Luminance step paradigm***
1251 In this paradigm (Fig. S1b), we used no textures at all. The screen was always a
1252 homogenous gray field, and the visual event of a "saccade" was replaced by an
1253 instantaneous step to a different gray value. The gray backgrounds had intensities
1254 between 30 and 90 (on our 8-bit projector). The instantaneous step in intensity caused
1255 either a positive contrast luminance step (in the range of +0.03 to +0.50 Michelson
1256 contrast) or a negative contrast luminance step (-0.03 to -0.50 Michelson contrast).
1257 This paradigm was used to characterize the stimulus-stimulus interactions that
1258 ultimately trigger retinal saccadic suppression (Figs. 4, 7, S8-10). We performed a total
1259 of 4 recordings (4 retinae from 4 mice) with this paradigm, always with the high density
1260 MaxOne MEA rig. A trial consisted of either 56 or 156 successive sequences

(Fig. S1b) that each combined a luminance step with a probe flash, as follows: there was first a “pre-step” fixation of 2 seconds where the retina was exposed to a fixed gray level (analogous to “pre-saccade” fixation in texture displacements), then an instantaneous switch to “post-step” fixation (analogous to “post-saccade”). At a certain time from the luminance step (delay: 17, 33, 50, 100, 250, 500, 1000 or 2000 ms), we presented a 2-frame (~33 ms) dark (-0.33 Michelson contrast) or bright (+0.33 Michelson contrast) probe flash. Some sequences contained no probe flash, the next luminance step then happened 4 seconds after the previous one. In a given experiment, we had 17 trials representing the 17 conditions: 8 flash delays x 2 probe flash polarities + 1 condition with no probe flash. Similar to the saccade paradigm, we always interleaved all conditions; that is, in any one of the 17 necessary trials, each luminance step could be followed by a bright or a dark probe at any of the 8 delays, or no probe flash. Moreover, we repeated the 17 trials at least 4 times.

A shorter version of this paradigm was used in our macaque retina recording (Fig. 7). Here, a trial consisted of 20 successive sequences. The 20 luminance steps induced contrasts in the range -0.5 to +0.5. Flashes of ~33 ms were presented with a delay of 17, 50, 100, 250, 500 and 2000 ms after the luminance step.

Other stimuli

Finally, we used other stimuli unrelated to the main experiments to help us characterize RGC properties (e.g. response polarity, latency, transiency, and spatial receptive fields). These stimuli had the same mean intensities and intensity ranges as the textures or luminance steps used in each experiment. Below, we describe these stimuli for the condition in which the texture intensities ranged from 0 to 60 pixel intensity (represented as grayscale RGB values in the units of our 8-bit projects). In experiments in which the textures ranged in intensity from 30 to 90, or the luminance step experiment, all intensities reported below were shifted upward by 30. (1) Full-field contrast steps. ON steps: stepping from 0 to 30 (+1 Michelson contrast) and from 30 to 60 (+0.33) for 2 s. OFF steps: stepping from 60 to 30 (-0.33) and from 30 to 0 (-1) for 2 s. (2) Full-field Gaussian flicker, 1 minute. Screen brightness was updated every frame and was drawn from a Gaussian distribution with mean 30 and standard deviation 9. This stimulus was used to calculate linear filters representing the temporal receptive fields of RGCs through reverse correlation (spike-triggered averaging of the

1293 stimulus history). (3) Binary checkerboard flicker, 10-15 minutes. The screen was
1294 divided into a checkerboard pattern; each checker either covered an area of
1295 55 x 55 μm, 60 x 60 μm, or 65 x 65 μm depending on the recording rig. The intensity
1296 of each checker was updated independently from the other checkers and randomly
1297 switched between 10 and 50 or 0 and 120. This stimulus also allowed us to calculate
1298 linear filters representing the spatial receptive fields of RGCs.

1299 **Visual stimuli: Cone photoreceptors imaging (Figs. 5, 6)**

1300 For cone imaging experiments, we used a minimalistic version of the luminance step
1301 paradigm used in retina electrophysiology. A homogeneous background alternated
1302 between a darker (pixel intensity 50 on 8-bit projector) and brighter gray value (pixel
1303 intensity 120 on 8-bit projector); the transitions between these two background values
1304 represented positive and negative contrast of 0.4 Michelson contrast. At various times
1305 after the luminance step (50, 250, and 2000 ms) we presented a probe flash (100 ms
1306 duration, +0.33 or -0.33 Michelson contrast). The probe flash at 2000 ms served as
1307 the baseline. The next background transition always happened 2 s after the preceding
1308 probe flash. The combination of the two luminance steps and the two probe flash
1309 polarities yielded a total of four combinations: negative-contrast luminance step
1310 followed by dark flash; negative-contrast luminance step followed by bright flash;
1311 positive-contrast luminance step followed by dark flash; and positive-contrast
1312 luminance step followed by bright flash. A single trial (Fig. S1c) was composed of the
1313 four step-flash combinations occurring three times (for the three delays with which the
1314 flash was presented); and the negative- and positive-contrast luminance step without
1315 a flash. Within a trial, these conditions were randomized. A trial was repeated three
1316 times. The luminance steps and the flashes were presented within a 700 μm disc
1317 region centered over the scan field.

1318 **Visual stimuli: Human psychophysics (Fig. 8)**

1319 In the human psychophysics experiment (Fig. 8), we mimicked the retinal luminance
1320 step experiments of Fig. 4. The paradigm (Fig. 8a) was similar to the one described in
1321 (Idrees et al., 2020). Subjects fixated a central fixation spot over a gray background
1322 that remained there for the entire duration of a trial. The background had one of 8

luminances (22.4, 30.24, 38.08, 45.92, 53.76, 61.6, 69.44, 77.28 cd m^{-2}). After a random initial fixation duration (800-1700 ms after fixation spot onset), the luminance of the background was changed suddenly (in one display frame update) to one of the remaining 7 luminances, inducing a positive-contrast luminance step or a negative-contrast luminance step. In our analysis, we used the luminance steps that induced contrasts in the range +0.3 to +0.56 Michelson contrast and -0.3 to -0.56 Michelson contrast. At one of 5 different possible times relative to the time of the luminance step (-24, -12, 36, 72, or 108 ms), a luminance pedestal (probe flash) was applied briefly for one display frame (~12 ms) at one of four locations relative to display center (7 deg above, below, to the right of, or to the left of center). Note that because the display was rasterized (that is, drawn by the computer graphics board from the top left corner in rows of pixels), the exact flash time and duration depended on the location of the flash on the display (but in a manner like other psychophysical experiments studying the same phenomenon, and also in a manner that is unlikely to affect our results). The luminance pedestal consisted of a square of 147.8 x 147.8 min arc, in which we added or subtracted a value to represent bright and dark probe flashes. We ensured that the contrast of the flash (relative to the currently displayed background luminance) was always the same across all trials: +0.033 for a bright flash, and -0.033 for a dark flash. Following each trial, the fixation spot was removed from the background to allow the subjects to relax. This inter trial period lasted for 500-1000 ms. The next trial happened consecutively, in a way that the current luminance of the background was used as the pre-step luminance. Subjects maintained fixation throughout all trials (except the inter trial period) and simply reported the locations of the brief flashes. Each subject performed 3 sessions, with 1120 trials per session.

Data Analysis

Data analysis: Retina electrophysiology

MEA recordings preprocessing

Low-density MEA recordings were high-pass filtered at a 500 Hz cutoff frequency using a tenth-order Butterworth filter. We extracted spike waveforms and times using thresholding, and we semi-manually sorted spikes using custom software. For high-density MEA recordings, we performed spike sorting by an offline automatic

1354 algorithm (Diggelmann et al., 2018) and assessed the sorted units using a custom
1355 developed tool, the UnitBrowser (Idrees et al., 2016). We judged the quality of all units
1356 using inter-spike intervals and spike shape variation. Low quality units, such as ones
1357 with high inter-spike intervals, missing spikes, or contamination, were discarded. All
1358 firing rate analyses were based on spike times of individual units. In total, we extracted
1359 3,510 high quality units after the spike sorting (referred to as RGCs from now on), from
1360 recordings of mouse retina. From pig retina recordings, we extracted 376 RGCs and
1361 from macaque retina we extracted 57 RGCs after the spike sorting. However, as we
1362 mention below, only a subset of these could be analyzed for saccadic suppression.

1363 ***RGCs characterization: Receptive fields, ON-OFF index, Transiency index***

1364 We first characterized the properties of RGCs. We calculated linear filters in response
1365 to full-field Gaussian flicker and binary checkerboard flicker by summing the 500-ms
1366 stimulus history before each spike. The linear filters allowed determining cell polarity.
1367 Specifically, the amplitude of the first peak of the filter was used: If the peak was
1368 positively deflected, the cell was categorized as an ON cell; if negatively deflected, the
1369 cell was an OFF cell. ON cells were later always analyzed with respect to their
1370 responses to bright probe flashes, and OFF cells were analyzed with dark probe
1371 flashes. We determined the spatial receptive fields of RGCs by calculating the linear
1372 filters for each region (checker) defined by the binary checkerboard flickering stimulus.
1373 The modulation strength of each linear filter, measured as the standard deviation (s.d.)
1374 along the 500 ms temporal kernel, is an estimate for how strongly that region drives
1375 ganglion cell responses. We fitted the resulting 2D-map of s.d. values with a two
1376 dimensional Gaussian and took the 2-σ ellipse (long axis) as the receptive field
1377 diameter. For all other figures and analyses, we converted spike times to estimates of
1378 firing rate by convolving these times with a Gaussian of σ = 10 ms standard deviation
1379 and amplitude 0.25 $\sigma^{-1}e^{1/2}$.

1380 For each RGC, we used responses to full-field contrast steps to calculate an ON-OFF
1381 index, a transiency index, and a response latency index. These indices were used to
1382 characterize the properties of RGCs that we included in our analyses. The ON-OFF
1383 index was calculated by dividing the difference between ON and OFF step peak
1384 response by their sum. The resulting index values ranged between -1 (OFF) and +1
1385 (ON) and were then scaled to span between 0 (OFF) and +1 (ON). The transiency

index was defined as the ratio of the response area within the first 400 ms and the total response area spanning 2000 ms. The resulting index had a value of 1 for pure transient cells. Response latency was calculated as the time from stimulus onset to 90% of peak response. This value was normalized to the maximum response latency in our dataset to create the response latency index.

Modulation index

To quantify retinal saccadic suppression, we first determined a baseline response, defined as the response to a probe flash approximately 2 s after texture displacement onset or 2 s after luminance step (delay between 1967 to 2100 ms, depending on the specific flash times used in a specific experiment). This baseline response was compared to responses of the same cell to the same flash when it occurred at an earlier time (i.e. closer in time to the "saccade"). Usually, the saccade-like texture displacements themselves caused significant neural responses (saccade-alone response, e.g. Fig. 1b), and the responses to the flashes were superimposed on these "saccade-responses". We therefore first isolated the component of the responses caused by the flashes by subtracting the saccade-alone responses from the composite saccade and flash responses. We refer to this isolated component as the flash-induced responses.

To get a robust estimate of the response to saccades-alone (i.e. without any flashes), we averaged spike rate from before saccade onset up until the next saccade onset for conditions in which no flash was presented, or until just before the flash onset for conditions in which a post-saccade flash was presented. This was done for each of the 39 successive saccades in a given trial.

We then computed a neural modulation index, ranging from -1 to +1. A value of -1 represents complete suppression of flash-induced responses, whereas +1 indicates "complete enhancement" of flash-induced responses (that is, there was only a response to a flash after saccades, but not to a flash in isolation). A modulation index of 0 meant no change in flash-induced response relative to the "baseline" response. The modulation index of an RGC for a given flash delay *d* after saccade onset was calculated as $(r_d - r_b)/(r_d + r_b)$ where r_d is the peak firing rate for the flash-component of the response (see above for how we isolated this from the composite saccade+flash

1417 response) and r_b is the peak firing rate for the baseline flash response (i.e. the same
1418 flash but occurring ~2 s away from any "saccade"; see above). In all cases, peak firing
1419 rate was estimated after averaging responses from all repetitions of a given condition
1420 (delay *d* or baseline) for a given RGC, across all saccades. For ON cells, the
1421 modulation index was based only on responses to bright flashes, and for OFF cells, it
1422 was based on responses to dark flashes. To quantify the modulation at a population
1423 level, we averaged the modulation indices of the individual RGCs in that population.
1424 For some analyses, we also calculated modulation indices of RGCs for each of the 39
1425 individual "saccades" using the same procedure.

1426 In some cells, individual saccades from the sequence of 39 were discarded. For
1427 example, imagine that "saccade No 3" gets discarded. This would happen when the
1428 baseline response strength (response to the probe flash with 2 s delay) after saccade
1429 No 3 is weak (specifically: peak amplitude less than 60% of the median of all 39
1430 baseline response strengths). We did this to ensure that our modulation indices were
1431 not marred by a denominator approaching zero (e.g. if both flash and baseline
1432 responses were weak). We did, however, re-include some sequences. For example,
1433 if the probe flash with delay 100 ms after saccade No 3 triggered a strong response
1434 (specifically: peak amplitude larger than the median baseline response peak across
1435 the 39 saccades), then saccade No 3 would be re-included for the condition "100 ms
1436 delay". This was done in order to re-include sequences (if discarded by the first step)
1437 for which the baseline flash response was weak but a flash after saccades nonetheless
1438 gave a robust response. For example, this could happen if a cell did not respond to
1439 the baseline flash but the saccade enhanced the response to a flash following it.

1440 Finally, to perform statistics, we applied tests both at the level of individual cells and
1441 at the level of the population. At the individual cell level, we determined whether the
1442 modulation index for a probe flash presented at a certain delay was significantly
1443 different from 0 (i.e. "Is the response of this cell modulated by the 'saccade'?"). For
1444 this, we performed a one-tailed sign test of the null hypothesis that the 39 individual
1445 modulation indices (or its subset in case weak sequences were discarded, as
1446 described above) came from a distribution with zero median. The alternative
1447 hypothesis was that the median was below (for negative modulation index) or above
1448 (for positive modulation index) zero. The modulation index was considered significant

1449 (i.e. the flash response was modulated by the saccade) at $p < 0.05$. However, we did
1450 not consider cells significantly modulated if the test had a power ($1-\beta$) smaller than
1451 0.8, which could happen if we previously had to exclude too many sequences ($N \leq 39$).
1452 At the population level, we determined whether the retinal output as a whole was
1453 modulated by saccades. For this, we performed a two-tailed Wilcoxon signed rank test
1454 of the null hypothesis that the median of the distribution of modulation indices did not
1455 differ from 0. Lastly, we tested whether the population modulation index was
1456 significantly different across populations of ON and OFF RGCs or across different
1457 paradigms. For this, we performed a two-tailed Wilcoxon rank-sum test of the null
1458 hypothesis that the median of the distribution of modulation indices did not differ
1459 across the two populations being tested.

1460 Since the modulation index was based on responses to the brief probe flashes, it could
1461 only be computed for RGCs that did respond to these brief flash stimuli. In our analysis,
1462 we included all such RGCs. Of the spike sorted RGCs across all paradigms, we
1463 included: 2002 of 3510 in mice; 228 of 376 in pigs; and 15 of 57 in macaque.

1464 ***Saccade (texture displacement) paradigm***

1465 Full-field saccades

1466 We analyzed 1010 mouse RGCs (633 ON; 377 OFF) and 228 pig RGCs (197 ON; 31
1467 OFF) for saccadic suppression using the full-field version of the saccade paradigm. A
1468 subset of data from 688 of the 1010 mouse RGCs and a subset of data from all the
1469 228 pig RGCs was presented previously (Idrees et al., 2020). Here, we perform novel
1470 analyses on the complete datasets from the RGCs recorded previously, in addition to
1471 analyzing the newly recorded RGCs. For each RGC, we quantified the modulation
1472 index for a full-field probe flash presented at different times from saccade onset.

1473 A subset of these RGCs were also tested for saccadic suppression while blocking
1474 GABAergic and glycinergic inhibition. For 82 ON and 30 OFF RGCs, we had a direct
1475 comparison with and without $GABA_{A,C}$ blockers (5 μM SR-9553 + 100 μM Picrotoxin)
1476 (Fig. 2c, S6a). For 51 ON and 13 OFF RGCs, we had a direct comparison with and
1477 without $GABA_{A,C}$ blockers in addition to glycine blocker (1μM Strychnine; Fig. 2d, S6b).

1478 In yet another subset of RGCs (72 ON; 49 OFF), we also analyzed saccadic
1479 suppression at scotopic light level (Fig. S4), which was 1 log unit dimmer than the light
1480 level at which all other recordings were performed. For these cells, we had a direct
1481 comparison of responses at scotopic and mesopic levels.

1482 Periphery saccades (global component of suppression)

1483 For each recorded RGC, we computed a masking factor (post hoc) to quantify how
1484 well its receptive field was covered by the 1000 x 1000 μm^2 mask. We first determined
1485 the spatial receptive field center of each RGC (described above in *RGCs*
1486 *characterization*). The masking factor was defined as the multiple of σ of the two
1487 dimensional Gaussian fit for which the ellipse just touched the mask boundary
1488 (Fig. S7d). Cells with receptive field centers within the mask were defined to have a
1489 positive masking factor while those lying outside were given a negative masking factor.
1490 The magnitude of the factor increased with distance from the edge of the mask. This
1491 way, cells for which the mask covered their receptive field centers and immediate
1492 surround had masking factors > 2 (these were the cells included in analysis shown in
1493 Figs. 2b, S5); cells with a mask covering only the receptive field center had masking
1494 factors between 1 and 1.5. Cells located close to the mask's edge, with masking
1495 factors between -1 to +1, had their receptive field centers partially exposed to the
1496 saccade. Finally, cells lying outside the mask where the receptive field center always
1497 experienced saccades had masking factors < -1. A total of 642 RGCs (401 ON; 241
1498 OFF) from 13 experiments were recorded with this spatial layout of the saccade
1499 paradigm. Cells for which clear receptive fields could not be calculated were excluded
1500 from any further analysis. The exact number of cells for different conditions within this
1501 paradigm are reported in the results section. For each RGC, we calculated the
1502 modulation index for flashes presented at different times from saccade onset, in the
1503 same manner as described under the heading *Modulation index*. Fig. S7e shows the
1504 modulation index of individual RGCs as a function of its masking factor. Only a subset
1505 of RGCs with masking factors in the range -3 to +5 were included in this analysis. The
1506 median modulation index was calculated by taking the median of modulation indices
1507 of RGCs within a 1.2 masking factor window, sampled at intervals of 0.1 (running
1508 median).

1509 In a subset of these experiments, we analyzed the effects of blocking GABAergic
1510 inhibition (using 5 μM SR-95531) on the modulation of probe flash responses in RGCs
1511 with masking factors > 2, i.e. with receptive field centers and immediate surround
1512 effectively masked. This included 62 ON RGCs and 35 OFF RGCs with robust
1513 responses to brief probe flashes with the pharmacological agent; only these RGCs
1514 were analyzed for saccadic suppression under the presence of SR-95531 (Fig. 2b). In
1515 a subset of these RGCs (29 ON; 25 OFF), we had a direct comparison of modulation
1516 indices with the control condition, i.e. periphery saccades in the absence of SR-95531
1517 (Fig. S5d).

1518 Checkerboard mask regions saccades

1519 In experiments where we investigated the local component of suppression
1520 (Figs. 2e-f, S7b, c), we had three stimulus presentation settings (Fig. S7a): (1)
1521 saccade and flash presented in all squares regions; (2, 3) saccades and flashes in
1522 alternate regions of a hypothetical binary checkerboard. For each recorded RGC we
1523 calculated the modulation index for the following two scenarios: saccades and flashes
1524 in all regions (Fig. S7a presentation setting 1); and saccades excluded from the
1525 receptive field center (Fig. S7a presentation setting 1 or 2 depending on the RGCs
1526 spatial position relative to the presentation area). For this, we first calculated the
1527 spatial receptive field center (see heading *RGCs characterization*; receptive field
1528 center was defined as the 1-σ ellipse of the 2D Gaussian fit) for each RGC. We then
1529 calculated the Euclidean distance between the receptive field center and the closest
1530 flash region for both presentation settings 2 and 3. For further analysis, we used the
1531 presentation setting with the shortest distance between a flash region and the
1532 receptive field center. In case this flash region is perfectly centered over the receptive
1533 field center, saccades will be excluded from a region of at most 300 μm diameter
1534 centered over the receptive field center. In most cases, the RGCs were indeed well
1535 centered within a flash region since the center of each region coincided with electrodes
1536 in the low density MEA. Nonetheless, for each RGC we calculated the intersection
1537 between its receptive field area and saccade regions in pixels (where each pixel
1538 corresponded to 3.75 μm on the retinal surface). RGCs for which more than 15% of
1539 their receptive field area intersected with the saccade regions were excluded from

1540 further analysis. In the end, a total of 51 RGCs (32 ON; 38 OFF) from 4 retinae
1541 recordings were used for further analysis of saccadic suppression.

1542 ***Luminance step paradigm***

1543 To quantify retinal "saccadic suppression" with the luminance-step paradigm (Fig. 4,
1544 Fig. 7), we used the same analyses and statistical procedures to those described
1545 above for the saccade (texture displacement) paradigm. The only difference was that
1546 instead of 39 successive sequences in a trial, we now had either 56 or 156 successive
1547 sequences (or 20 in case of macaque retina experiment), spanning a contrast range
1548 of ±0.03 to ±0.5 Michelson contrast. Similar to the texture displacement paradigms,
1549 the modulation index was based on responses to brief probe flashes (~33 ms flash
1550 duration), and it could therefore only be computed for cells that did respond to these
1551 flash stimuli (N = 366 of 668 spike sorted RGCs from 4 mouse retinae; N = 15 of 57
1552 spike sorted RGCs from a macaque retina). The modulation index for ON RGCs
1553 (N = 259 mouse RGCs; N = 13 macaque RGCs) was calculated from responses to
1554 bright probe flashes, and that for OFF RGCs (N = 107 mouse RGCs; N = 2 macaque
1555 RGCs) was calculated from responses to dark flashes. A subset of data from all mouse
1556 RGCs was presented previously (Idrees et al., 2020). Here, we perform novel analyses
1557 on the complete dataset of the same RGCs.

1558 In a subset of luminance step experiments (2 mouse retinae), we analyzed the effects
1559 of blocking GABAergic and glycinergic inhibition on the modulation of probe flash
1560 responses. 115 ON RGCs showed robust responses to the brief probe flashes with
1561 and without the pharmacological blockers. However, none of the OFF RGCs
1562 responded robustly to the baseline probe flash in the presence of pharmacological
1563 blockers and therefore OFF RGCs were excluded in quantification of saccadic
1564 suppression in the presence of pharmacological blockers.

1565 We also analyzed if the modulation of flash-induced responses depended on the
1566 strength of the response to the preceding luminance step. This analysis was done to
1567 establish whether suppression of flash responses resulted from saccade-induced
1568 saturation or adaptation of ganglion cell responses (Fig. S10). For each RGC, we
1569 calculated an association index which quantified the monotonic relationship between
1570 response to the luminance step and response to subsequent flashes. We first binned

1571 the responses across the 56 or 156 step-flash sequences (Fig. S1b) based on the
1572 contrast induced by the luminance step in each sequence. Bin width was set to 0.025
1573 Michelson contrast. Then, within each bin, we averaged the responses to luminance
1574 steps alone (Fig. S9a, b, top row) and to luminance steps followed by probe flashes.
1575 For each probe flash delay and contrast bin, we quantified the strength of the response
1576 induced by the luminance step preceding each probe flash (we integrated the average
1577 response to the luminance steps followed by probe flashes, up until the response to
1578 that probe flash). The modulation index was calculated as usual. We then calculated
1579 the Spearman's rank correlation coefficient (R) between the modulation index and the
1580 response strength induced by the luminance step, across all the contrast bins. This
1581 can be visualized from the insets in Fig. S9. For ease in interpretation of the results,
1582 we termed the resulting correlation coefficient as the association index. Intuitively, this
1583 association index describes the monotonic relationship between the step response
1584 strength and the strength of suppression and can be interpreted as follows: the larger
1585 the magnitude of the association index, the stronger is the monotonic relation between
1586 the two quantities. A negative value indicates that stronger step responses are
1587 associated with decreasing (more negative) modulation indices (i.e. weaker flash
1588 responses → suppression). A positive value indicates that stronger step responses
1589 are associated with increasing modulation indices (i.e. stronger flash responses →
1590 less suppression or even enhancement). In the example cell of Fig. S9a, the
1591 association index has large negative values for flashes immediately after the positive
1592 luminance step, suggesting that a stronger step response is indeed strongly correlated
1593 with stronger suppression of subsequent flashes. A robust calculation of association
1594 index was only possible for luminance steps that activated the RGC (i.e.
1595 positive-contrast luminance steps in ON RGCs, negative-contrast luminance steps in
1596 OFF RGCs). Fig. S10 shows the association index for each RGC and flash time as a
1597 function of the cell's modulation index.

1598 In Fig. 6f, we plot modulation index as a function of RGC transiency index (see heading
1599 *RGCs characterization* for details on transiency index). The RGCs shown in this
1600 sub-figure were a subset of the RGCs analyzed with the luminance step paradigm for
1601 which we could also compute a transiency index. The relation between RGC
1602 transiency and modulation index for each condition was modeled using a linear

1603 regression least-squares fit through the ON and OFF RGC population. To determine
1604 if the slope of the resulting line was statistically significant non-zero, we conducted a
1605 t-test of this slope.

1606 **Data analysis: Cone photoreceptors**

1607 ***Quantifying cone responses***

1608 We analyzed data from 11 scan fields recorded from four retinae (2 mice). Each scan
1609 field was 128 x 128 pixels, which on the retinal surface was 94 x 94 μm^2,
1610 110 x 110 μm^2, or 132 x 132 μm^2, depending on the zoom factor used. In each scan
1611 field, we identified regions of interest (ROIs) as a group of neighboring pixels with
1612 correlated fluorescence signals in time. Only ROIs with diameters corresponding to
1613 the cone axon terminal diameter (3-7 μm) were considered for further analysis. The
1614 output signal of the ROIs (baseline normalized iGluSnFR indicator fluorescence
1615 signal), represented the changes in glutamate release at the cone terminals. A total of
1616 931 ROIs were extracted from the 11 scan fields. Identifying the ROIs and extracting
1617 their output signal were automated using custom IGOR Pro scripts.

1618 Within a scan field, each ROI was sampled every 256 ms (3.9 Hz sampling rate). This
1619 interval was greater than the duration of probe flashes (100 ms) in these experiments.
1620 Therefore, the measured signal of many ROIs might not capture the peak response to
1621 the probe flashes. A conventional upsampling method, such as interpolation, could
1622 also underestimate the peak response in this case. However, since all ROIs (within
1623 and across scan fields) experienced the same visual stimulus (Fig. S1c), but were
1624 sampled at different points in time, we temporally 'stitched' the output from these ROIs.
1625 The resulting signal had a sampling interval of 2 ms, where the signal in a specific time
1626 bin was computed from ROIs sampled within that specific time window. In this
1627 'stitching' approach, we first baseline-adjusted the output signal of each ROI for a trial
1628 by subtracting the baseline activity (calculated as the average ROI output across 1 s
1629 epoch prior to the first luminance step in the trial). Then, for each 2-ms time bin, we
1630 averaged the response across those ROIs that were sampled within that time window.
1631 This resulted in an output vector of the same duration as the trial but with a sampling
1632 interval of 2 ms. The output vector was empty for time bins where no ROIs were
1633 sampled. We therefore convolved this output vector with a moving average filter of

size 80 ms to fill in the empty time bins and to also smooth out the stitching boundaries (boundaries between time bins filled with output from different ROIs). This method gave a much better temporal resolution than conventional upsampling techniques, robustly capturing the peak for the 100 ms duration probe flash, as shown in Fig. 5b.

The 'stitched' signal was then cut into snippets that captured the relevant responses to our stimulus (e.g. step followed by probe flash). For this, we used stimulation trigger signals that marked the presentation of each luminance step. Each snippet was then baseline-adjusted by subtracting the average response over 800 ms prior to the luminance step. This way the output signal was 0 prior to a luminance step (Fig. 5). The output was averaged across the three repetitions of the trial. The normalized and averaged snippets represented the cone response to a particular stimulus sequence (for example Fig. 5a) and were used to fit parameters for model cones as described in the next section.

RGC model

To describe cone responses (Fig. 5) and RGC responses (Fig. 7) to our luminance step paradigm, we used a phenomenological model of the retina, previously published in Drinnenberg et al., 2018.

The original model related light intensity to retinal ganglion spiking activity by three layers of processing: first, the "light stimulus" was passed to model cone photoreceptors. Their activity was modulated by negative feedback from model horizontal cells. Second, the output of the model cones was passed to six inner retina pathways describing retinal processing by three different ON and three different OFF bipolar cells (fast, intermediate and slow pathways). Third, the output from the model pathways were then fed into model RGCs to yield RGC spiking activity. This cascade modeled RGC spiking in response to the "light stimulus" passed to model cones.

The cone responses were describes as

$$r(t) = \frac{\alpha_c y(t)}{[1 + \beta_c z(t)]} - h(t) \qquad \text{(Equation 2)}$$

where

$$r(t) = V(t) - V_{dark} \qquad \text{(Equation 3)}$$

$V(t)$ and V_{dark} were the instantaneous and dark membrane potentials of the cone, respectively, $h(t)$ was the feedback signal from the horizontal cell, and α_c and β_c were numerical factors. The time-varying functions $y(t)$ and $z(t)$, were related to light input through linear convolution, as

$$y(t) = \int_{-\infty}^{t} dt' K_y(t - t') I(t') \qquad \text{(Equation 4)}$$

$$z(t) = \int_{-\infty}^{t} dt' K_z(t - t') I(t') \qquad \text{(Equation 5)}$$

where $I(t)$ was the incident light intensity (or, more precisely, R*/s). The kernels describing the cone response were given by

$$K_y(t) = \frac{t}{\tau_y} \frac{e^{-\frac{t}{\tau_y}}}{\tau_y} \qquad \text{(Equation 6)}$$

and

$$K_z(t) = \gamma K_y(t) + (1 - \gamma) \frac{t}{\tau_z} \frac{e^{-\frac{t}{\tau_z}}}{\tau_z} \qquad \text{(Equation 7)}$$

where τ_z was larger than τ_y, and $0 \leq \gamma \leq 1$ ensured proper normalization. Note that $\int_0^{\infty} dt' K_y(t - t') = 1$ for all filters. The response of the horizontal cell was described by

$$h(t) = \alpha_c \int_{-\infty}^{t} dt' K_h(t - t') r(t') \qquad \text{(Equation 8)}$$

with

$$K_h(t) = \frac{t}{\tau_h} \frac{e^{-\frac{t}{\tau_h}}}{\tau_h} \qquad \text{(Equation 9)}$$

Here, instead of the cone model parameters used in the published model (Drinnenberg et al., 2018), we re-fitted the parameters of the model cone to reflect our measured data of cone output (Fig. 5b) which yielded faithful fits (Fig. S12) to our experimentally measured cone responses.

All the parameters of the outer retina component (Equations 2 and 8) of our circuit model were fit once to cone responses (Fig. 5b, S11) and then kept unchanged for all simulations reported in Fig. 6. The fitted values are given as follows (original values (Drinnenberg et al., 2018) are reported in brackets):

$\alpha_c = -3.342 * 10^{-5}\ (-9.602 * 10^{-6}), \beta_c = -1.273 * 10^{-6}\ (-1.148 * 10^{-5}), \gamma = 0.842\ (0.764), \alpha_h = 0.016\ (0.177), \tau_y = 48.98\ ms\ (50.64), \tau_z = 200ms\ (576.9), \tau_h = 1.232 * 10^3 ms\ (371).$

The small α_h suggested that in our cone recordings, horizontal cell feedback had only a minor effect.

In (Drinnenberg et al., 2018) three different retinal pathways were modelled according to

$$b_{p,k}(t) = \left\lfloor -1^k \left(\int_{-\infty}^{t} dt' K_p(t-t') V(t') - \theta_{p,k} \right) \right\rfloor \qquad \text{(Equation 10)}$$

where $p = 1,2,3$ labeled the pathway based on its response properties (1 = fast, 2 = intermediate, 3 = slow), $k = 0$ for OFF pathways and $k = 1$ for ON pathways.

$$\lfloor x \rfloor = \begin{cases} 0, & x < 0 \\ x, & x \geq 0 \end{cases} \qquad \text{(Equation 11)}$$

was a thresholding non-linearity, and $\theta_{p,k}$ acted as a threshold.

The main difference between the pathways was the temporal characteristics of the filters K_p. In the current study we wanted to smoothly vary the transiency of the model ganglion cells. To this end, we based our bipolar pathway on the fast bipolar pathway $(p = 1)$ and modified its temporal characteristics to make it less transient. K_1 represented a high-pass filter which took the derivative of the cone potential on the order of 1 ms. We obtained K_1 by convolving the high-pass filter of the form

$$\mathrm{G}(t) = \sin\left(\frac{\pi t}{\mu}\right)\frac{1}{\sqrt{2\pi}\sigma}e^{-\frac{1}{2}\left(\frac{t-\mu}{\sigma}\right)^2}, with\ \mu = 3\ ms, \sigma = 1\ ms \qquad \text{(Equation 12)}$$

with an exponential function.

$$K_1(t) = \int_{-\infty}^{t} dt' \left(e^{-\frac{t-t'}{\tau_d}}\right) G(t') \qquad \text{(Equation 13)}$$

Higher values of the time constant, τ_d, of the exponential function decreased the pathway transiency. We set $\tau_d = 0.5$ as the default transient pathway (Fig. 6a-d). The 'transiency parameter' shown in In Fig. 6e was obtained by normalizing $15 \geq \tau_d \geq 0.5$ in the range 0 to 1, with 0 being less transient. In the original model (Drinnenberg et al., 2018), $K_1(t) = G(t)$.

The threshold $\theta_{1,k}$ was set to $-1^k \cdot 0.1$.

$b_{1,k}(t)$, the output of fast inner retina models was used as the input to the model RGCs used in this study. The spiking rate of the model RGC was obtained as the thresholded input and a temporally coarse version of the input's derivative,

$$R_{1,k}(t) = \left\lfloor (1-\alpha) b_{1,k}(t) + \alpha \left(\int_{-\infty}^{t} dt'\, K(t-t')\, b_{1,k}(t')\right) - \theta \right\rfloor \qquad \text{(Equation 14)}$$

where $K(t)$ was a biphasic filter similar in its form to $G(t)$. The threshold, θ, was a multiple of the peak response to any given input. We used the same parameters for the inner retina component as the ones described in the published model (Drinnenberg et al., 2018):

(i) $Transient\ OFF,\ R_{1,0}(t)\colon \alpha = 0,\ \theta = 0;$

(ii) $Transient\ ON, R_{1,1}(t)\colon \alpha = 0, \theta = 0;$

All simulations were computed with a 1 ms sampling interval.

Using the above cascade, we calculated model RGC's spike rate in response to the recorded cone output when subjected to "luminance steps alone" and "luminance

steps followed by probe flash" stimuli (Fig. 6a, b). Similar to real RGC analysis, we calculated the "flash-induced responses" (Fig. 6c) by subtracting "response to luminance steps alone" (Fig. 6a) from "response to luminance steps followed by probe flash" (Fig. 6b). We then calculated the modulation index also in the same way as for the real RGCs: $(r_d - r_b)/(r_d + r_b)$ where r_d was the peak spiking rate of the flash-induced response for the flash presented with delay d from the luminance step, and r_b was the peak firing rate for the baseline flash-induced response (flash at 2000 ms).

As a control, we replaced the model cone responses with the experimentally acquired cone responses (Fig. 5) thus forming a hybrid model. Before passing the cone response to the downstream model pathways, we passed it through a low pass filter to further smooth the fluctuations at the stitching boundaries in order to avoid discontinuities in calculation of its temporal derivative. For this smoothing, we convolved the cone output with a moving average filter of size 40 ms. Here, the model ON RGC responses (Fig. S12a, b, columns 1-2) were calculated using the cone responses to bright probe flashes (Fig. 5a, b, columns 1-2), and OFF RGC responses (Fig. S12a, b, columns 3-4) were calculated using cone responses to dark probe flashes (Fig. 5a, b, columns 3-4). The resulting hybrid model RGC responses (Fig. S12) were consistent with the pure model responses shown in Fig. 6.

Data analysis: Human psychophysics

We analyzed eye movements in all trials and detected saccades using established methods (Chen and Hafed, 2013). We excluded from analysis trials in which a saccade or microsaccade happened anywhere in the interval from 200 ms before to 50 ms after a probe flash. At each flash time, we calculated the proportion of correct trials to obtain time courses of this perceptual measure. We obtained time course curves for each subject individually, and then averaged it across trials and different contrasts of the luminance steps. Reduced proportion of correct trials at any flash time indicated perceptual saccadic suppression. A subset of data from 4 of the 5 subjects was used in our previous study (Idrees et al., 2020). Here we perform novel analyses of the complete dataset.

We applied a two-tailed Wilcoxon rank-sum test to determine if the suppression after luminance steps differed across bright and dark probe flashes.

All data analyses were performed in MATLAB (The MathWorks Inc).

1765 ## References

1766 Amthor, F.R., Tootle, J.S., and Gawne, T.J. (2005). Retinal ganglion cell coding in
1767 simulated active vision. Vis. Neurosci. *22*, 789–806.

1768 Appleby, T.R., and Manookin, M.B. (2019). Neural sensitization improves encoding
1769 fidelity in the primate retina. Nat. Commun. *10*, 1–15.

1770 Baccus, S.A., Olveczky, B.P., Manu, M., and Meister, M. (2008). A Retinal Circuit
1771 That Computes Object Motion. J. Neurosci. *28*, 6807–6817.

1772 Barlow, H.B., Derrington, A.M., Harris, L.R., and Lennie, P. (1977). The effects of
1773 remote retinal stimulation on the responses of cat retinal ganglion cells. J. Physiol.
1774 *269*, 177–194.

1775 Baylor, D.A., and Hodgkin, A.L. (1974). Changes in time scale and sensitivity in turtle
1776 photoreceptors. J. Physiol. *242*, 729–758.

1777 Beeler, G.W. (1967). Visual threshold changes resulting from spontaneous saccadic
1778 eye movements. Vision Res. *7*, 769–775.

1779 Berry, M., Brivanlou, I., Jordan, T., and Meister, M. (1999). Anticipation of moving
1780 stimuli by the retina. Nature *398*.

1781 Breitmeyer, B. (2007). Visual masking: Past accomplishments, present status, future
1782 developments. Adv. Cogn. Psychol. *3*, 9–20.

1783 Bremmer, F., Kubischik, M., Hoffmann, K.P., and Krekelberg, B. (2009). Neural
1784 dynamics of saccadic suppression. J. Neurosci. *29*, 12374–12383.

1785 Chen, C.-Y., and Hafed, Z.M. (2013). Postmicrosaccadic enhancement of slow eye
1786 movements. J. Neurosci. *33*, 5375–5386.

1787 Chen, C.-Y., and Hafed, Z.M. (2017). A neural locus for spatial-frequency specific
1788 saccadic suppression in visual-motor neurons of the primate superior colliculus. J.
1789 Neurophysiol. *117*, 1657–1673.

1790 Chen, E.Y., Marre, O., Fisher, C., Schwartz, G., Levy, J., da Silviera, R.A., and
1791 Berry, M.J. (2013). Alert response to motion onset in the retina. J. Neurosci. *33*,

1792 120–132.

1793 Chichilnisky, E.J., and Baylor, D.A. (1999). Receptive-field microstructure of blue-
1794 yellow ganglion cells in primate retina. Nat. Neurosci. *2*, 889–893.

1795 Chichilnisky, E.J., and Kalmar, R.S. (2002). Functional asymmetries in ON and OFF
1796 ganglion cells of primate retina. J. Neurosci. *22*, 2737–2747.

1797 Clark, D.A., Benichou, R., Meister, M., and Azeredo da Silveira, R. (2013).
1798 Dynamical Adaptation in Photoreceptors. PLoS Comput. Biol. *9*.

1799 Dalkara, D., Byrne, L.C., Klimczak, R.R., Visel, M., Yin, L., Merigan, W.H., Flannery,
1800 J.G., and Schaffer, D. V. (2013). In vivo-directed evolution of a new adeno-
1801 associated virus for therapeutic outer retinal gene delivery from the vitreous. Sci.
1802 Transl. Med. *5*.

1803 Diamond, M.R., Ross, J., and Morrone, M.C. (2000). Extraretinal control of saccadic
1804 suppression. J. Neurosci. *20*, 3449–3455.

1805 Diggelmann, R., Fiscella, M., Hierlemann, A., and Franke, F. (2018). Automatic spike
1806 sorting for high-density microelectrode arrays. J. Neurophysiol. *120*, 3155–3171.

1807 Drinnenberg, A., Franke, F., Morikawa, R.K., Jüttner, J., Hillier, D., Hantz, P.,
1808 Hierlemann, A., Azeredo da Silveira, R., and Roska, B. (2018). How Diverse Retinal
1809 Functions Arise from Feedback at the First Visual Synapse. Neuron 1–18.

1810 Duffy, F.H., and Lombroso, C.T. (1968). Electrophysiological evidence for visual
1811 suppression prior to the onset of a voluntary saccadic eye movement. Nature *218*,
1812 1074–1075.

1813 Enroth-Cugell, C., and Jakiela, H.G. (1980). Suppression of cat retinal ganglion cell
1814 responses by moving patterns. J. Physiol. *302*, 49–72.

1815 Euler, T., Hausselt, S.E., Margolis, D.J., Breuninger, T., Castell, X., Detwiler, P.B.,
1816 and Denk, W. (2009). Eyecup scope—optical recordings of light stimulus-evoked
1817 fluorescence signals in the retina. Pflügers Arch. - Eur. J. Physiol. *457*, 1393–1414.

1818 Euler, T., Franke, K., and Baden, T. (2019). Studying a light sensor with light:
1819 Multiphoton imaging in the retina. Neuromethods *148*, 225–250.

1820 Farrow, K., Teixeira, M., Szikra, T., Viney, T.J., Balint, K., Yonehara, K., and Roska,
1821 B. (2013). Ambient illumination toggles a neuronal circuit switch in the retina and
1822 visual perception at cone threshold. Neuron *78*, 325–338.

1823 Field, G.D., Sher, A., Gauthier, J.L., Greschner, M., Shlens, J., Litke, A.M., and
1824 Chichilnisky, E.J. (2007). Spatial properties and functional organization of small
1825 bistratified ganglion cells in primate retina. J. Neurosci. *27*, 13261–13272.

1826 Frey, U., Egert, U., Heer, F., Hafizovic, S., and Hierlemann, A. (2009).
1827 Microelectronic system for high-resolution mapping of extracellular electric fields
1828 applied to brain slices. Biosens. Bioelectron. *24*, 2191–2198.

1829 Fried, S., Münch, T., and Werblin, F. (2002). Mechanisms and circuitry underlying
1830 directional selectivity in the retina. Nature 411–414.

1831 Garvert, M.M., and Gollisch, T. (2013). Local and global contrast adaptation in retinal
1832 ganglion cells. Neuron *77*, 915–928.

1833 Geffen, M.N., De Vries, S.E.J., and Meister, M. (2007). Retinal ganglion cells can
1834 rapidly change polarity from off to on. PLoS Biol. *5*, 0640–0650.

1835 Gollisch, T. (2013). Features and functions of nonlinear spatial integration by retinal
1836 ganglion cells. J. Physiol. Paris *107*, 338–348.

1837 Hafed, Z.M. (2013). Alteration of Visual Perception prior to Microsaccades. Neuron
1838 *77*, 775–786.

1839 Hafed, Z.M., and Krauzlis, R.J. (2010). Microsaccadic suppression of visual bursts in
1840 the primate superior colliculus. J. Neurosci. *30*, 9542–9547.

1841 Ibbotson, M.R., Crowder, N.A., Cloherty, S.L., Price, N.S.C., and Mustari, M.J.
1842 (2008). Saccadic modulation of neural responses: possible roles in saccadic
1843 suppression, enhancement, and time compression. J. Neurosci. *28*, 10952–10960.

1844 Idrees, S., Franke, F., Diggelmann, R., Hierlemann, A., and Münch, T.A. (2016).
1845 UnitBrowser - A tool to evaluate and post-process units sorted by automatic spike
1846 sorting algorithms. Front. Neurosci. *10*.

1847 Idrees, S., Baumann, M.P., Franke, F., Münch, T.A., and Hafed, Z.M. (2020).

1848 Perceptual saccadic suppression starts in the retina. Nat. Commun. *11*, 1977.

1849 Itokazu, T., Hasegawa, M., Kimura, R., Osaki, H., Albrecht, U.-R., Sohya, K.,
1850 Chakrabarti, S., Itoh, H., Ito, T., Sato, T.K., et al. (2018). Streamlined sensory motor
1851 communication through cortical reciprocal connectivity in a visually guided eye
1852 movement task. Nat. Commun. *9*, 338.

1853 Kemmler, R., Schultz, K., Dedek, K., Euler, T., and Schubert, T. (2014). Differential
1854 regulation of cone calcium signals by different horizontal cell feedback mechanisms
1855 in the mouse retina. J. Neurosci. *34*, 11826–11843.

1856 Khabou, H., Desrosiers, M., Winckler, C., Fouquet, S., Auregan, G., Bemelmans,
1857 A.P., Sahel, J.A., and Dalkara, D. (2016). Insight into the mechanisms of enhanced
1858 retinal transduction by the engineered AAV2 capsid variant -7m8. Biotechnol.
1859 Bioeng. *113*, 2712–2724.

1860 Kleiser, R., Seitz, R.J., and Krekelberg, B. (2004). Neural correlates of saccadic
1861 suppression in humans. Curr. Biol. *14*, 386–390.

1862 Krekelberg, B. (2010). Saccadic suppression. Curr. Biol. *20*, R228–R229.

1863 Krishnamoorthy, V., Weick, M., and Gollisch, T. (2017). Sensitivity to image
1864 recurrence across eye-movement-like image transitions through local serial inhibition
1865 in the retina. Elife e22431.

1866 Krueger, J., and Fischer, B. (1973). Strong periphery effect in cat retinal ganglion
1867 cells. Excitatory responses in ON- and OFF-center neurones to single grid
1868 displacements. Exp. Brain Res. *18*, 316–318.

1869 Li, P.H., Field, G.D., Greschner, M., Ahn, D., Gunning, D.E., Mathieson, K., Sher, A.,
1870 Litke, A.M., and Chichilnisky, E.J. (2014). Retinal Representation of the Elementary
1871 Visual Signal. Neuron *81*, 130–139.

1872 Lin, B., and Masland, R.H. (2006). Populations of wide-field amacrine cells in the
1873 mouse retina. J. Comp. Neurol. *499*, 797–809.

1874 Litke, A.M., Bezayiff, N., Chichilnisky, E.J., Cunningham, W., Dabrowski, W., Grillo,
1875 A. a., Grivich, M., Grybos, P., Hottowy, P., Kachiguine, S., et al. (2004). What does

1876 the eye tell the brain?: Development of a system for the large-scale recording of
1877 retinal output activity. IEEE Trans. Nucl. Sci. *51*, 1434–1440.

1878 Marvin, J.S., Borghuis, B.G., Tian, L., Cichon, J., Harnett, M.T., Akerboom, J.,
1879 Gordus, A., Renninger, S.L., Chen, T.W., Bargmann, C.I., et al. (2013). An optimized
1880 fluorescent probe for visualizing glutamate neurotransmission. Nat. Methods *10*,
1881 162–170.

1882 Matin, E. (1974). Saccadic suppression: a review and an analysis. Psychol. Bull. *81*,
1883 899–917.

1884 Mayo, J.P., and Sommer, M.A. (2008). Neuronal Adaptation Caused by Sequential
1885 Visual Stimulation in the Frontal Eye Field. J. Neurophysiol. *100*, 1923–1935.

1886 Müller, J., Ballini, M., Livi, P., Chen, Y., Radivojevic, M., Shadmani, A., Viswam, V.,
1887 Jones, I.L., Fiscella, M., Diggelmann, R., et al. (2015). High-resolution CMOS MEA
1888 platform to study neurons at subcellular, cellular, and network levels. Lab Chip *15*,
1889 2767–2780.

1890 Münch, T.A., da Silveira, R.A., Siegert, S., Viney, T.J., Awatramani, G.B., and
1891 Roska, B. (2009). Approach sensitivity in the retina processed by a multifunctional
1892 neural circuit. Nat. Neurosci. *12*, 1308–1316.

1893 Noda, H., and Adey, W.R. (1974). Excitability Changes in Cat Lateral Geniculate
1894 Cells during Saccadic Eye Movements. Science (80-.). *183*, 543–545.

1895 Ölveczky, B.P., Baccus, S.A., and Meister, M. (2003). Segregation of object and
1896 background motion in the retina. Nature *423*, 401–408.

1897 Passaglia, C.L., Freeman, D.K., and Troy, J.B. (2009). Effects of remote stimulation
1898 on the modulated activity of cat retinal ganglion cells. J. Neurosci. *29*, 2467–2476.

1899 Reinhard, K., Tikidji-Hamburyan, A., Seitter, H., Idrees, S., Mutter, M., Benkner, B.,
1900 and Münch, T.A. (2014). Step-By-Step instructions for retina recordings with
1901 perforated multi electrode arrays. PLoS One *9*, e106148.

1902 Roska, B., and Werblin, F. (2003). Rapid global shifts in natural scenes block spiking
1903 in specific ganglion cell types. Nat. Neurosci. *6*, 600–608.

1904 Ross, J., Morrone, M.C., Goldberg, M.E., and Burr, D.C. (2001). Changes in visual
1905 perception at the time of saccades. Trends Neurosci. *24*, 113–121.

1906 Sakatani, T., and Isa, T. (2007). Quantitative analysis of spontaneous saccade-like
1907 rapid eye movements in C57BL/6 mice. Neurosci. Res. *58*, 324–331.

1908 Schiller, P.H. (1968). Single unit analysis of backward visual masking and
1909 metacontrast in the cat lateral geniculate nucleus. Vision Res. *8*, 855–866.

1910 Schreyer, H.M., and Gollisch, T. (2020). Nonlinearities in retinal bipolar cells shape
1911 the encoding of artificial and natural stimuli. BioRxiv 1–40.

1912 Schütz, A., Braun, D., and Gegenfurtner, K. (2011). Eye movements and perception:
1913 A selective review. J. Vis. *11*, 1–30.

1914 Schwartz, G.W., Okawa, H., Dunn, F. a, Morgan, J.L., Kerschensteiner, D., Wong,
1915 R.O., and Rieke, F. (2012). The spatial structure of a nonlinear receptive field. Nat.
1916 Neurosci. *15*, 1572–1580.

1917 Shapley, R., and Enroth-Cugell, C. (1984). Chapter 9 Visual adaptation and retinal
1918 gain controls. Prog. Retin. Res. *3*, 263–346.

1919 Szatko, K.P., Korympidou, M.M., Ran, Y., Berens, P., Dalkara, D., Schubert, T.,
1920 Euler, T., and Franke, K. (2020). Neural circuits in the mouse retina support color
1921 vision in the upper visual field. Nat. Commun. *11*, 3481.

1922 Tatler, B.W., Wade, N.J., Kwan, H., Findlay, J.M., and Velichkovsky, B.M. (2010).
1923 Yarbus, Eye Movements, and Vision. Iperception. *1*, 7–27.

1924 Tikidji-Hamburyan, A., Reinhard, K., Seitter, H., Hovhannisyan, A., Procyk, C.A.,
1925 Allen, A.E., Schenk, M., Lucas, R.J., and Münch, T.A. (2015). Retinal output
1926 changes qualitatively with every change in ambient illuminance. Nat. Neurosci. *18*,
1927 66–74.

1928 Volkmann, F.C. (1986). Human visual suppression. Vision Res. *26*, 1401–1416.

1929 Wei, W. (2018). Neural mechanisms of motion processing in the mammalian retina.
1930 Annu. Rev. Vis. Sci. *4*, 165–192.

1931 Werblin, F. (2010). Six different roles for crossover inhibition in the retina: correcting
1932 the nonlinearities of synaptic transmission. Vis. Neurosci. *27*, 1–8.

1933 Wurtz, R.H. (2008). Neuronal mechanisms of visual stability. Vision Res. *48*, 2070–
1934 2089.

1935 Yarbus, A.L. (1967). Eye Movements and Vision (Boston, MA: Springer US).

1936 Zaghloul, K.A., Manookin, M.B., Borghuis, B.G., Boahen, K., and Demb, J.B. (2007).
1937 Functional circuitry for peripheral suppression in Mammalian Y-type retinal ganglion
1938 cells. J Neurophysiol *97*, 4327–4340.

1939 Zhang, Y., Kim, I.-J., Sanes, J.R., and Meister, M. (2012). The most numerous
1940 ganglion cell type of the mouse retina is a selective feature detector. Proc. Natl.
1941 Acad. Sci. *109*, E2391–E2398.

1942 Zuber, B.L., and Stark, L. (1966). Saccadic suppression: Elevation of visual
1943 threshold associated with saccadic eye movements. Exp. Neurol. *16*, 65–79.

1944